Mapping Discomfort through Patient Input in Robotic Physiotherapy

Jevon Ravenberg

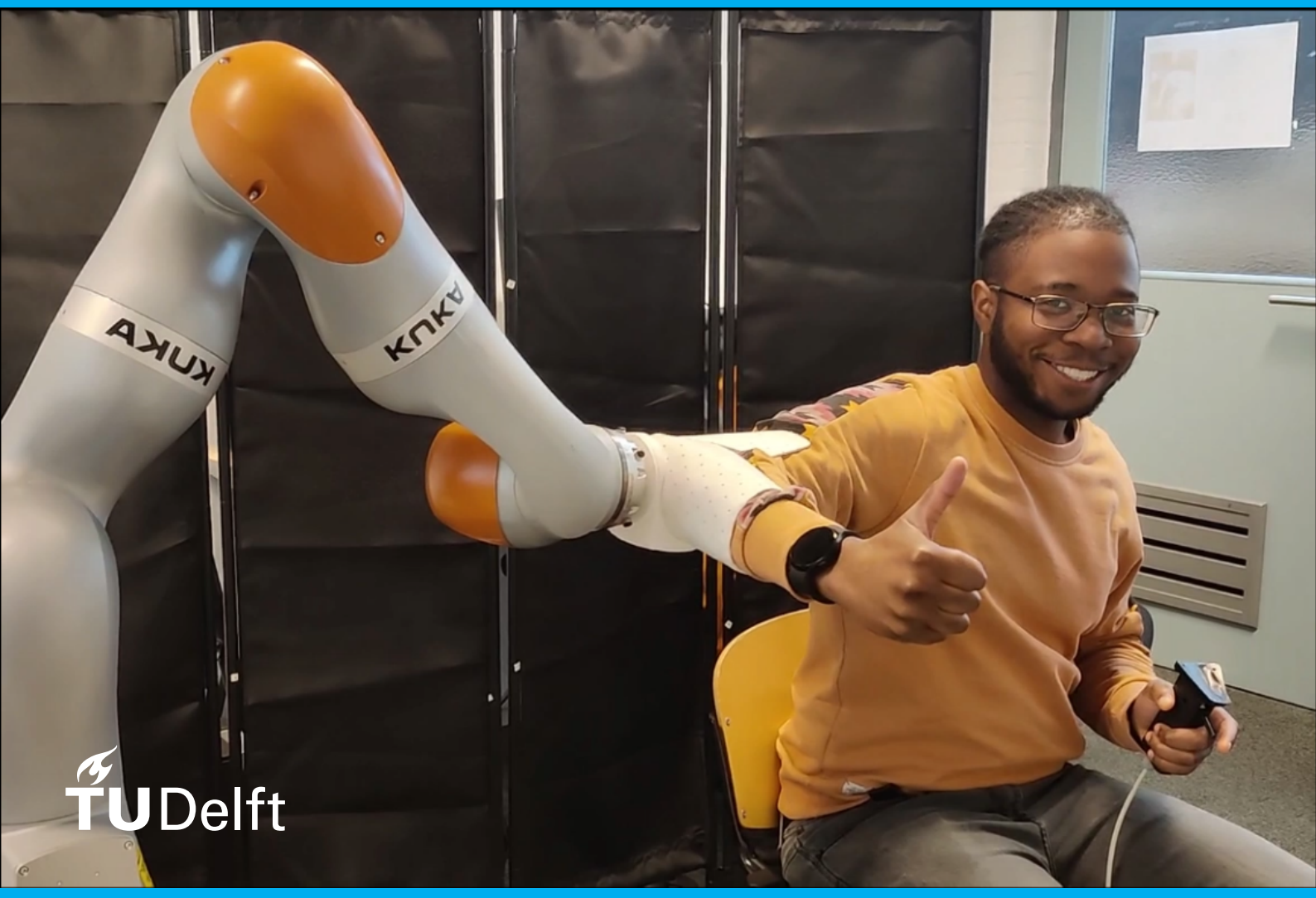

Mapping Discomfort through Patient Input in Robotic Physiotherapy

by

Jevon Ravenberg

to obtain the degree of Master of Science
at the Delft University of Technology,
to be defended publicly on Wednesday January 24, 2024 at 11:00 AM.

Student number: 4896270
Project duration: March 20, 2023 – January 24, 2024
Thesis committee:

Dr. ir. L. Peternel,	TU Delft, supervisor, chair
Dr. I. Belli,	TU Delft, member, supervisor
Dr. C. Della Santina,	TU Delft, member
Dr. ir. A. Stienen,	TU Delft, member

TU Delft

Preface

I am happy to finally present my final thesis report. Over these past months I have learned a lot about robot physiotherapy, working with KUKA robot arms, and research in general.

I would like to thank my supervisors, Luka Peternel and Italo Belli, for their invaluable guidance and support during my thesis. They were always ready to help and stimulated me to do better. I would also like to thank the rest of the PT Bot team, Micah Prendergast and Ajay Seth, for their help in brainstorming and finding solutions to problems I encountered during the thesis. I want to thank Leandro de Souza Rosa and Rodrigo Perez Dattari for their advice and support for controlling the robot. And of course, I would also like to thank Cosimo Della Santina and Arno Stienen for making time to review my thesis as committee members.

Finally, I would like to thank my friends and family for supporting me in both my personal life and my research, and all the participants in my study for their time and willingness to participate in my experiment.

Jevon Ravenberg
Delft, January 2024

Contents

1

Paper

Mapping Discomfort through Patient Input in Robotic Physiotherapy

Jevon Ravenberg
Supervised by: Italo Belli and Luka Peternel

***Abstract*—In this work, we propose a method of processing patient input on discomfort level during robot shoulder physiotherapy into discomfort maps. These maps represent the patient's discomfort distribution throughout the range of motion of the shoulder, interpretable by both physiotherapists and robots. This method consists of three parts: the patient can input discomfort with a linear push-button; a collaborative robot arm is used to track the motion of the patient's shoulder; and audiovisual feedback of inputted discomfort is given to the patient and the therapist. The method was validated in human factors experiments simulating shoulder physiotherapy sessions, where the subject is tasked with recreating a reference discomfort map through an auditory reference signal that emulates this discomfort. Here the robot also acts as the physiotherapist, moving the subject's shoulder. The signal is a beeping sound, whose rate scales with the discomfort intensity at the measured pose in the reference discomfort map. We performed experiments with a total of 10 participants, demonstrating the viability of our method during patient-robot interaction. The results we collected also highlighted the presence of a time delay between the discomfort signal and the user input, and its effect on discomfort maps.**

I. Introduction

Musculoskeletal injuries resulting from accidents, recreational activities, and general wear-and-tear due to aging are the primary contributors to disability and work impairment. Among these injuries, a shoulder rotator-cuff (RC) tear stands out as one of the most prevalent, with an estimated prevalence rate of 22.1% in the general population and over 50% for individuals aged 60 and above [2]. Restoring shoulder mobility and functionality after RC injuries requires a patient to undergo a prolonged and costly physiotherapy process.

Due to the intricate nature of the shoulder joint and a lack of quantitative insights into the risks of re-injury, conventional practices in RC physiotherapy tend to be conservative, even when administered by expert physiotherapists [3]. This conservative approach limits the treatment intensity in terms of range of motion (RoM), potentially slowing down the healing process. Increasing RoM safely, however, can enhance recovery speed and recovery completeness [4]. Additionally, RC therapy itself can be physically demanding for physiotherapists who typically have to handle many patients a day, one at a time. This is exacerbated by the growing gap between the amount of people with rehabilitative needs and physiotherapists, caused among others by the ageing population and decreasing growth of medical personnel [5]. Robotic-assisted rehabilitation can offer solutions to these problems.

These robotic platforms can help reduce physical load on the physiotherapist by taking over the weight of the patient's arm, and through telerehabilitation [6] the therapist is capable of administering physiotherapy remotely and to multiple people at once. Furthermore, robotic platforms can quantify the patient's condition and incorporate this into its control system and communicate this to the therapist. For instance, the muscle effort of the patient can be estimated from electromyography (EMG) measurements [7], [8]. However, this only gives a limited insight into the inner workings of the musculoskeletal system, similar to how human physiotherapists have limited insight. Using musculoskeletal models, however, can give an accurate estimate of the actual internal properties of the human body, such as joint loading [9], muscle fatigue [10], muscle comfort [11], and muscle manipulability [12].

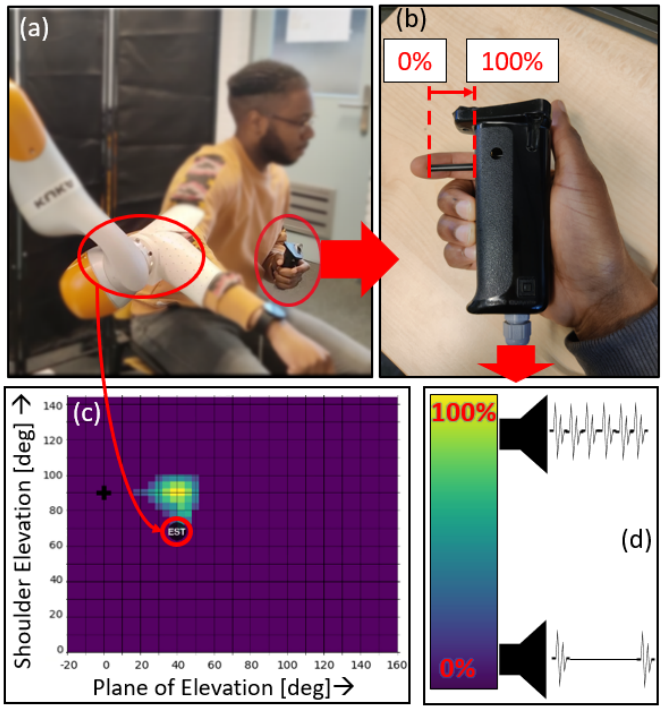

Fig. 1: Overview of the discomfort map creation system. (a) A KUKA LBR iiwa 7 R800 robotic manipulator [1] moves along with the patient's shoulder through an elbow brace and estimates their shoulder state. (b) The push-button interface used to input the patient's discomfort intensity, held by the free arm. (c) The discomfort map created by the patient. (d) The audio feedback is a beeping sound. As the input discomfort intensity increases, the time between beeps decreases. Note: Image (a) is mirrored for demonstration purposes.

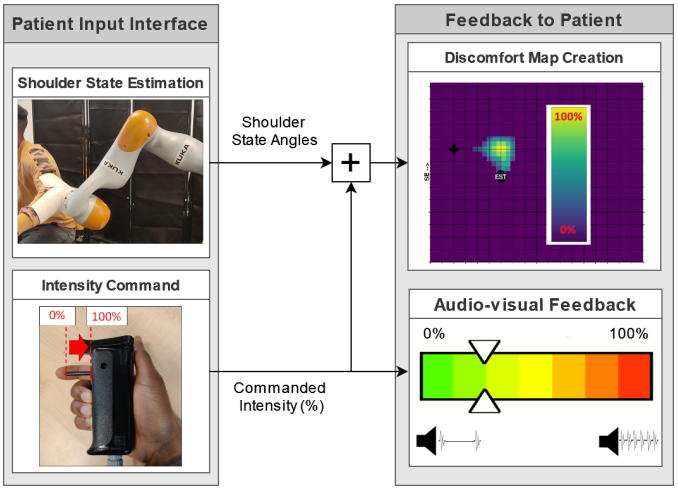

Fig. 2: Workflow of the system for creating discomfort maps. It consists of two main sections: patient input and feedback to the patient. The patient input consists of their shoulder state estimated by the robot and their discomfort intensity commanded with the push-button. The feedback to the patient consists of their drawn discomfort map and audio-visual feedback of their commanded intensity. When drawing the map the patient places down blobs centered at the shoulder state, whose shape depends on the commanded intensity.

The previous work presented in [13], [14] uses a musculoskeletal model of the patient's shoulder to estimate the safe RoM, defined as the movement region where the strain in the RC tendons is limited to safe levels. Rather than using this model during operation, this safe region is pre-computed and abstracted into "strain maps" which provide an intuitive representation of the RC tendon strains to the physiotherapist that can also be used for effective real-time control.

However, a major shortcoming of robot-assisted physiotherapy is the decrease in contact and communication between the physiotherapist and their patient. This makes it harder for the therapist to monitor the condition of the patient, i.e., whether they are in pain. While musculoskeletal models give insight into musculoskeletal sources of pain, e.g., the strain maps giving insight into muscle strain, they cannot quantify pain itself. This is because pain can have many different sources and the experience of pain is deeply personal and characterized by a tremendous variability between individuals [15], thus what makes one person feel excessive pain may not be exactly the same for another.

Conversely, it is possible to estimate the patient's pain. Pain responses include changes in physiological markers such as blood pressure, heart rate and skin conductance, which can be measured [16]; and behavioral responses such as facial expressions, which can be used with machine learning to detect pain [17]. Though in literature, these methods are most often validated through comparison with a subjective numerical rating from the patient, e.g., the Numerical Rating Scale (NRS) [18]. So in order to supplement the robotic system with information about the patient's pain distribution, the most straightforward manner would be to simply ask the patient's opinion.

To address the problem of the strain maps lacking information about the patient's pain distribution, we propose a new method of integrating patient input on discomfort with patient state estimation during robotic physiotherapy, in order to create "discomfort maps". Through a handheld push-button interface, the patient can input their discomfort level in real-time during the therapy session. These discomfort maps represent the discomfort distribution experienced by the patient over the RoM of the therapy. The main advantages of this method are that it is intrinsically personalized to the patient and requires a simple pipeline that outputs directly usable quantitative information. See Fig. 1 for an overview of the system. The discomfort maps can be used with strain maps to not only avoid high-strain shoulder poses but also shoulder poses the patient has deemed uncomfortable, and are especially useful for telerehabilitation, where the physiotherapist is not physically present to monitor the patient's demeanor.

There is precedent for allowing the patient to input their pain level using a handheld interface. Studies in [19] and [20] used devices with a slider as the input interface. This allows for precise input but requires visual attention and the use of both hands. Studies in [21] and [22] used grip devices as the input interface. These are single-handed and more intuitive to use but need to be calibrated to the patient. The push-button interface used in our proposed method combines the single-handed, intuitive nature of the grip interfaces with the more precise position-based and non-personalized input of the slider. Furthermore, none of those studies were able to build state-space maps like our approach can, since they lack a motion-tracking component.

This study presents the discomfort maps, demonstrates how they are generated, and discusses insights gained from validation through human factors experiments that emulate robotic shoulder physiotherapy. During the experiments, subjects will

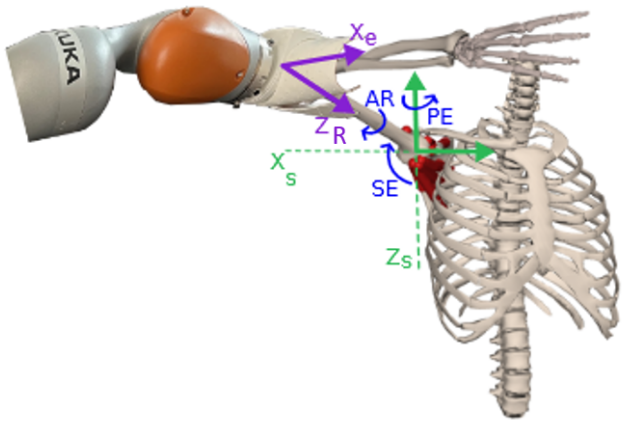

Fig. 3: Overview of the coordinate systems used: the shoulder frame (green), with the origin centered on the glenohumeral joint; DoF of the glenohumeral joint (blue); robot's end-effector frame (purple). When the patient is wearing the arm brace, the elbow frame coincides with the end-effector frame.

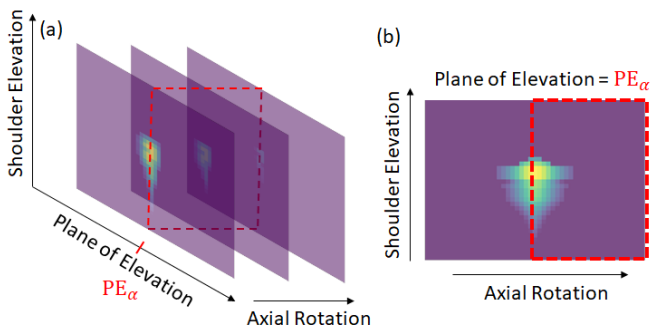

Fig. 4: (a) Discomfort maps for multiple values of AR layered on each other. (b) Cross-sectional view of the bounded area in (a). The plane of elevation is at a fixed value of PE$_\alpha$. This shows how the intensity dampens along the shoulder elevation and plane of elevation, but also along the axial rotation.

be tasked with recreating a reference discomfort map using only a discomfort-emulating reference signal in the form of audio. A KUKA LBR iiwa 7 R800 collaborative robot arm [1] will serve as the robotic physiotherapist, guiding the shoulder through specific trajectories.

II. Methodology

The overview for our proposed method is shown in Fig. 2. Discomfort maps represent the patient's discomfort distribution across the entire RoM of their shoulder. They are created by combining the patient's shoulder state with their input on discomfort level over time. Shoulder state estimation is performed by a collaborative robot arm, which can also move the patient's shoulder through set trajectories. For inputting discomfort level, the patient uses a push-button interface, which is accompanied by audio-visual feedback for ease of use.

The methodology is split into three subsections. Section II-A details the shape and creation process of discomfort maps. Section II-B discusses the interface used for inputting discomfort level and explains the audio-visual feedback interface to the patient. Finally, Section II-C describes the robot controller. Details on the shoulder state estimation are excluded from this section for brevity, but can be found in Section A of the appendix.

A. Discomfort Map

The discomfort maps show the patient's discomfort intensity level over the entire RoM of the shoulder. Because the discomfort maps were conceived as an addition to strain maps from previous work [13], [14], the definition of shoulder state and the shape of the maps are maintained. The shoulder state is defined as the state of the glenohumeral joint, i.e., the motion of the humerus (upper arm bone) relative to the scapula (shoulder blade), which has 3 degrees of freedom (DoF). As such the shoulder state vector is defined as

$$\boldsymbol{\alpha} = [\text{AR PE SE}], \tag{1}$$

where AR $\in[-90°, 90°]$ is the axial rotation, PE $\in [-20°, 160°]$ is the shoulder plane of elevation, and SE $\in [0°, 144°]$ is the shoulder elevation. This is also shown in Fig. 3. The state $[0°, 0°, 0°]$ coincides with the neutral pose where the arm rests at the side. Similar to strain maps, the shoulder range is discretized in 4° increments.

For visualisation purposes the 3D map of the patient's discomfort intensity level across AR, PE, and SE is represented as multiple layers of 2D maps, where AR is fixed. A single discomfort map shows the patient's discomfort intensity across PE and SE for a fixed AR, but by layering discomfort maps for all values of AR the entire shoulder RoM is spanned (see Fig. 4).

The idea behind the map creation is that the patient indicates points of discomfort and the intensity of this discomfort. It can be assumed that not only the indicated point, i.e., shoulder pose, is uncomfortable, but also poses around it to a lesser degree. This range should increase with intensity, because a point with high intensity most likely has a larger area of effect. So the patient places down 3D ellipsoidal "blobs" in the discomfort maps that scale in amplitude and size with the commanded intensity and are centered around their current shoulder state; AR determines the layer, while PE and SE determine the position on that layer.

This leads to the following technical implementation, where the intensity at each point in the discomfort maps over time is given by:

$$I(t, \boldsymbol{\alpha}) = \max\left(I(t-1, \boldsymbol{\alpha}),\ \ f(t, \boldsymbol{\alpha})\right), \tag{2}$$

$$f(t, \boldsymbol{\alpha}) = i(t) \prod_{j \in A} \exp\left(-\frac{1}{2}\left(\frac{\boldsymbol{\alpha}_j - \boldsymbol{\mu}_j(t)}{\boldsymbol{\sigma}_j(t)}\right)\right), \tag{3}$$

$$A = \{\text{AR, PE, SE}\},$$

$$\boldsymbol{\sigma}(t) = i(t)\frac{1}{4}[w_{AR}\ w_{PE}\ w_{SE}], \tag{4}$$

where $I(t, \boldsymbol{\alpha})$ is the intensity in the discomfort maps at shoulder state $\boldsymbol{\alpha}$ at time t, $f(t, \boldsymbol{\alpha})$ describes the intensity distribution of the newest blob, i is the intensity commanded by the patient as a percentage, $\boldsymbol{\mu}$ is the estimated patient shoulder state, and w_j is the width of the blob at 100% intensity in the j-direction, with $[w_{AR}\ w_{PE}\ w_{SE}] = [60°\ 25°\ 25°]$.

Eq. (3) shows that the blobs are shaped like a Gaussian function, i.e., the intensity is highest at the center and decreases to 0 at the boundary. From Eq. (4) follows that the width of the blob is approximated as 4 times the standard deviation of the Gaussian function[1]. The blob width is larger in the AR direction due to the fact that a rotation in AR corresponds to a relatively smaller movement of the arm compared to equivalent rotations in PE and SE. This adjustment aims to prevent the patient from inadvertently leaving a discomfort region through such a minor movement. Eq. (2) describes how the discomfort intensity in a point can only be overwritten by a blob with higher intensity in that point. This stems from a conservative

[1]For a normalized Gaussian function f centered at 0, $f(\pm 2\sigma) \simeq 0.135$. In our software implementation, values below this threshold could be disregarded for efficiency.

approach that regards the highest commanded intensity in a point as representative.

B. Patient Input and Feedback Interfaces

The interface used for inputting discomfort intensity must enable the patient to instantly indicate not only whether and when they experience discomfort but also to accurately specify the level of discomfort. Furthermore, the interface should be comfortable to hold for a long time and intuitive. That is why for this method a handle with a spring-return push-button is used. This device has been repurposed from [23]. The discomfort intensity commanded to the system scales linearly with the position of the push-button, e.g., fully pushed in is 100% and fully extended, so relaxed, is 0%. The handle is held in the free arm, to prevent the effects of involuntary muscle contractions due to the therapy on the button-press.

When the patient is focused on physiotherapy it can be easy to lose track of the discomfort intensity they are commanding to the system, decreasing accuracy. In order to resolve this issue, visual feedback of the commanded intensity is given through a color bar, where the pointer moves along with the intensity, on a monitor in front of the patient. This is also useful for the physiotherapist because they otherwise would not be able to clearly see what the patient is inputting. The setup also includes auditory feedback of the commanded intensity in the shape of a beeping sound, whose rate is proportional to this intensity. Although primarily designed for the experiments (refer to Section III-B), this auditory feedback can be repurposed to provide feedback to the physiotherapist through an alternative sense when visual attention is otherwise engaged.

C. Robot Control

The robot arm is not only used to estimate the shoulder state of the subject through encoder measurements, but also to move the subject's shoulder through set trajectories. For this, an impedance controller is used, which takes the desired motion of the robot end-effector as an input and outputs the robot joint torques based on mass-spring-damper equations [24]. This means the impedance is characterized by virtual inertia, stiffness, and damping terms. Unlike fully stiff conventional position-controlled robots, the torque-controlled robot with an end-effector impedance controller can be complaint, which is crucial for safe human-robot interaction. The robot end-effector force and corresponding torques that generate that force are calculated with:

$$\boldsymbol{F} = \boldsymbol{K}(\boldsymbol{X_r} - \boldsymbol{X}) - \boldsymbol{D}(\dot{\boldsymbol{X}}_r - \dot{\boldsymbol{X}}) \tag{5}$$

$$\boldsymbol{\tau} = \boldsymbol{J}^T \boldsymbol{F} \tag{6}$$

where $\boldsymbol{F} \in \mathbb{R}^6$ is the output force, $\boldsymbol{K} \in \mathbb{R}^{6\times6}$ is the Cartesian stiffness matrix, $\boldsymbol{D} \in \mathbb{R}^{6\times6}$ is the Cartesian damping matrix, $\boldsymbol{X}_r \in \mathbb{R}^6$ is the Cartesian reference end-effector pose, $\boldsymbol{X} \in \mathbb{R}^6$ is the current end-effector pose of the robot, $\boldsymbol{J} \in \mathbb{R}^{6\times7}$ is the robot Jacobian, which describes the relationship between end-effector velocities and joint velocities, and $\boldsymbol{\tau} \in \mathbb{R}^7$ is the commanded robot joint torques. The system is critically damped so $\boldsymbol{D} = 2\sqrt{\boldsymbol{K}}$ [25].

The robot arm has 7 joints, thus 7 DoF, while the end-effector has 6 DoF. This means that the robot arm has redundant joints and as a result, it can have the same end-effector pose in many different joint configurations. To ensure repeatability, a null space controller is also employed [26], which makes it so the robot will always have a proclivity for a selected joint configuration. The null space controller is described by:

$$\boldsymbol{\tau} \mathrel{+}= (\boldsymbol{I} - \boldsymbol{J}^T \boldsymbol{J}^{+T})(\boldsymbol{P}_N(\boldsymbol{q}_r - \boldsymbol{q}) - \boldsymbol{D}_N(\dot{\boldsymbol{q}})) \tag{7}$$

where $\boldsymbol{I} \in \mathbb{R}^{7\times7}$ is the identity matrix, $\boldsymbol{J}^+ \in \mathbb{R}^{7\times6}$ is the Moore-Penrose pseudo-inverse of the Jacobian $\boldsymbol{J}$, $\boldsymbol{P}_N \in \mathbb{R}^{7\times7}$ is the proportional gain of the controller, $\boldsymbol{D}_N \in \mathbb{R}^{7\times7}$ is the derivative gain (damping), $\boldsymbol{q}_r \in \mathbb{R}^7$ is the reference joint configuration, and $\boldsymbol{q} \in \mathbb{R}^7$ is the current joint configuration of the robot. The system is critically damped so $\boldsymbol{D}_N = 2\sqrt{\boldsymbol{P}_N}$.

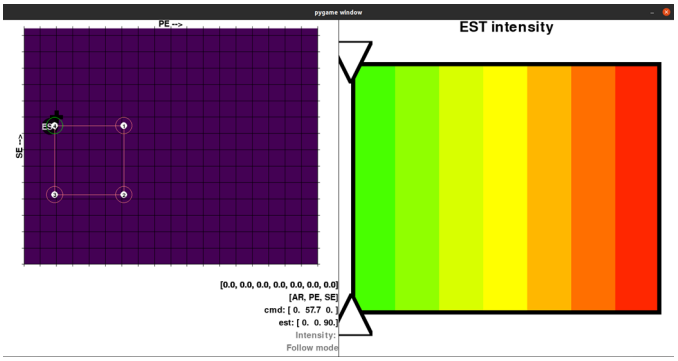

Fig. 5: Visual interface for the experiments. The left pane shows the subject's estimated shoulder state as a black circle in the map. This pane can also display the discomfort map created by the subject, the reference discomfort map, and the corresponding reference shoulder trajectory (as is currently shown in pink). The right pane shows the color bar for feedback on the subject's commanded discomfort intensity, the pointer (white triangles) move to the right as intensity increases.

III. Experiments and Results

The presented research was approved by the TU Delft Human Research Ethics Committee (HREC). The experiments can be separated into two main parts:

- the functionality test (Section III-C), with the goal of demonstrating the discomfort map creation process;
- the human factors experiments (Section III-D), with the goal of analysing the practicality of the proposed method on untrained subjects.

For HREC approval, we could not inflict actual (physical) discomfort on the subjects to generate discomfort maps in the human factors experiments. Instead, the subject is asked to recreate a reference discomfort distribution translated to a discomfort map, using the proposed method in a simulated physiotherapy session, where their shoulder is moved by the robot arm. The subject is not able to see the reference map, but is instead given a reference signal based on this map, which

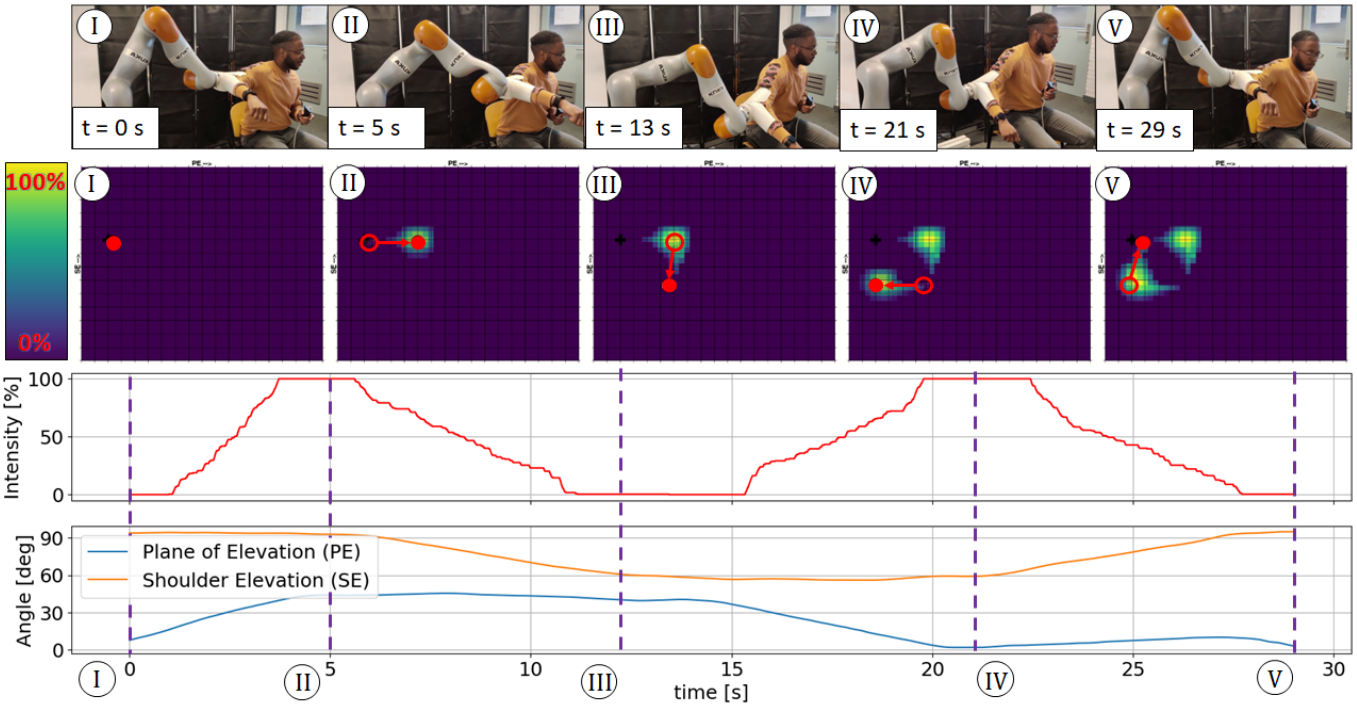

Fig. 6: Demonstration of discomfort map creation using the proposed method, with snapshots taken at specific timestamps A to E. The first row shows the robot and subject poses at these timestamps. The second row shows the discomfort map at these timestamps, with the current shoulder state marked as a filled red dot and the previous as a non-filled circle. The third row shows the discomfort intensity commanded by the subject over time, i.e., how much the push-button is pressed. The fourth row shows the PE and SE angles over time. AR is missing from this overview, because for this demonstration the estimated AR is locked to 0. Note: The images in the first row are mirrored for demonstration purposes.

emulates discomfort. This signal was chosen to be a beeping sound pattern, further explained in Section III-B. The results of the human factors experiments are discussed in Section III-E. For these experiments, 10 healthy participants, 8 male and 2 female, in the age range of 20-30 were selected. As required by the HREC approval, all participants had to give informed consent beforehand.

A. Experimental setup

The general setup for the experiments is the same (see also Fig. 1): the subject is seated in a chair, adjustable in height, with their left elbow fitted in the elbow brace attached to the end-effector of the robot arm. This brace locks the elbow in a 90° bend. The starting shoulder state for every experiment is [AR PE SE] = [0° 0° 90°], where the bent arm is parallel to the horizontal plane (see picture I in Fig. 6). The elbow brace is made of a soft molded thermoplastic attached to a solid 3D-printed base. As a safety measure, these two parts detach with enough force. The robot arm used is a KUKA LBR iiwa 7 R800 collaborative robot arm [1]. The arm is impedance controlled, details of which were discussed in Section II-C. The discomfort intensity input interface is the push-button as described in Section II-B. The subject receives visual feedback on their estimated shoulder state, the robot's reference trajectory, and their commanded discomfort intensity through a monitor (see Fig. 5). This window is created in Pygame and runs at 60 FPS on average. The subject receives the auditory signal on discomfort intensity through Bluetooth headphones with unnoticeable latency.

For all the experiments, AR was locked to 0°, unless stated otherwise. This means the discomfort map related processes were restricted to a single layer, significantly reducing the complexity of the experiments. Furthermore, the RoM was restricted to PE$\leq$60° and SE$\geq$30°, because the robot could not physically follow the subject's arm for shoulder states beyond these limits.

B. Discomfort-emulating Auditory Signal Protocol

As stated before, for the human factors experiments the subject is given a signal that emulates the reference discomfort intensity from the reference discomfort map. The most appropriate medium for conveying this signal was determined to be auditory over visual or tactile, from the following considerations:

- the average simple reaction time, i.e., the reaction time in experiments where there is only one stimulus and one response, is longest for visual stimuli with 180-200 ms and shortest for auditory stimuli with 140-160 ms [27]–[29]. Touch stimuli is intermediate with 155 ms [30]. This difference persists when the subject is asked to give more complex responses [31], [32]. Though our experiments here cannot be classified as simple reaction

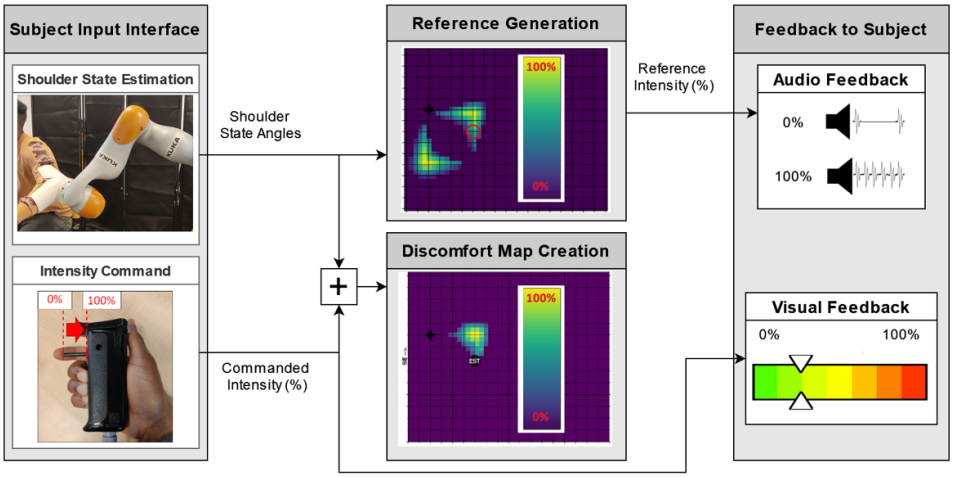

Fig. 7: System workflow for human factors experiments, where the subject is tasked with recreating a reference discomfort map. The system consists of four main sections: subject input, reference generation, discomfort map creation, and feedback to the subject. The subject input consists of their shoulder state estimated by the robot and their discomfort intensity commanded with the push-button. The reference discomfort intensity is generated from the intensity in the reference map at the current estimated shoulder state. This reference intensity is modulated to an audio signal: faster beeping for higher intensity. The feedback to the subject consists of this audio signal and visual feedback of the subject's commanded intensity. When drawing the discomfort map the user places down blobs centered at their current estimated shoulder state, whose shape depends on the commanded intensity. The drawn discomfort map is not shown to the subject.

experiments, it can be concluded that the reaction time in our experiments would be lowest for auditory and tactile signals.

- the haptic system for tactile signals can be designed in a way to closely mimic the discomfort that may arise during real shoulder physiotherapy, however this is much more difficult to implement than auditory (and visual) signals.

In order to convey changes in reference intensity, the auditory signal can vary in frequency, volume or rate. Volume modulation is not appropriate, because humans do not perceive loudness linearly, and rate modulation is significantly easier to implement than frequency modulation. Thus, the auditory signal is implemented as a repeating 1 kHz beep sound. The time between beeps is inversely proportional to the reference intensity:

$$t = (1 - i_r) + t_0 \tag{8}$$

where t is the time between beeps, t_0 is duration of the beep itself, with $t_0 = 0.3$ seconds, and i_r is the reference intensity as a percentage. This reference intensity is the intensity in the reference map at the current estimated shoulder state.

C. Functionality Test

The goal of the functionality test is to demonstrate the discomfort map creation process of our method in AR, PE and SE directions. Fig. 2 gives an overview of the system. For the functionality test the robot is fully compliant, i.e., $\boldsymbol{K} = \boldsymbol{P}_N = \mathbf{0}$ (see Eqs. (5) and (7)), and because there is no reference map in this case, the auditory signal is controlled by the subject's commanded intensity instead, i.e., $i_r = i$ (see Eq. (8)).

Fig. 6 shows a demonstration of the discomfort map creation functionality of the proposed method. This figure however is limited to a single layer, i.e., it only shows the motion tracking of the system in the PE and SE directions, and AR is explicitly locked to 0°, meaning the map is locked to a single layer. Appendix B shows a similar demonstration, but without an AR lock, focusing on movement in AR instead, while keeping PE and SE steady. It can be seen that as AR changes, the map-drawing continues on a new layer. Video of these demonstrations is shown in [33]. The demonstrations show how the method can be used to produce discomfort maps, depicting the discomfort intensity across the DoF of the glenohumeral joint: AR, PE, and SE.

D. Human Factors Experiments

The goal of the human factors experiments is analysing the practicality of the proposed method on untrained subjects. Fig. 7 gives a general overview of the system. In order to manage the complexity of the experiments, AR was locked to 0°, meaning analysis is restricted to a single discomfort map. Because we cannot inflict real discomfort on subjects, they are instead asked to recreate a reference discomfort map without being able to see it, from the reference auditory signal described in Section III-B, in a simulated robotic physiotherapy session.

The experiments were split into two tasks:

- Task I, where the robot arm is omitted, instead the subject's shoulder trajectory is simulated by the reference trajectory, and the subject is only asked to follow the reference auditory signal with the push-button;
- Task II, where the robot arm guides the subject's shoulder through a reference trajectory and the subject is asked to correct errors in the robot's trajectory while simultaneously following the reference auditory signal with the push-button.

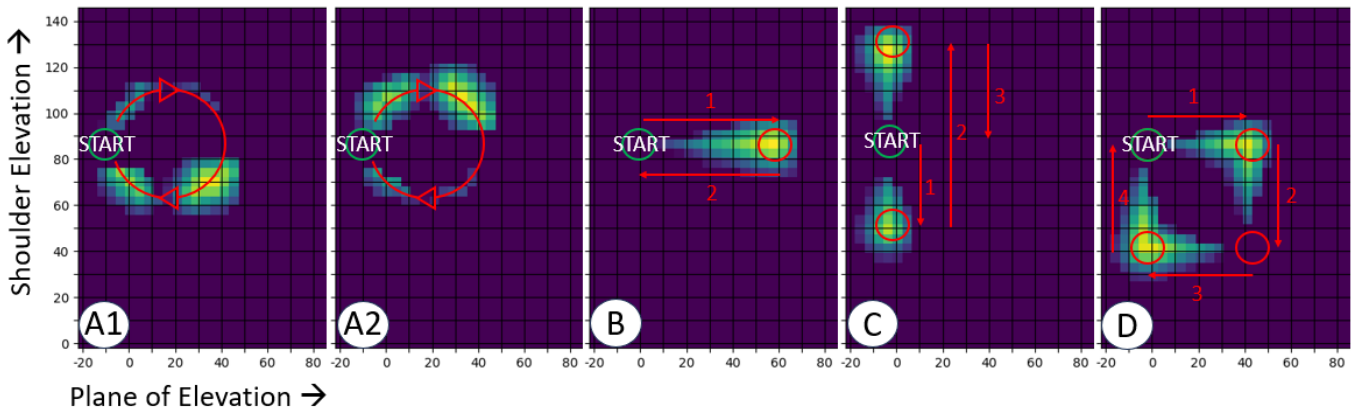

Fig. 8: The reference maps used for the human factors experiments and their accompanying trajectories.

TABLE I: Structure of human factors experiments ordered from left to right.

Reference	A1	A2	B	C	D
Task	I	I	II	II	II
# Trials	3	3	5	5	5
Average trial duration (s)	30	30	13	20	20

The purpose of Task I is to study the tracking of the auditory reference signal in isolation and to prepare the subjects for Task II. The purpose of Task II aligns more closely with the goal of the human factors experiments, which is to study the practicality of the proposed method in a simulated robotic physiotherapy session.

The experiments are structured as follows. It starts with a familiarization period, where the subject can freely use the push-button. Here, the auditory signal is controlled by their button-press. This way they can develop a mapping between the button-press, the color bar for visual feedback, and the beeping speed of the signal. This is necessary for the rest of the experiment, where the subject needs to match their button-press to the signal instead. The subject is allowed as much time as they require for familiarization. This is followed by Task I, then Task II. The reference maps and corresponding trajectories (henceforth collectively referred to as "reference") used for the tasks are shown in Fig. 8, labeled A1, A2, B, C, and D. The structure for the rest of the experiment is shown in Table I. It can be seen that in Task II the references gradually increase in complexity. Multiple references are used and the number of trials per reference is limited to prevent the subjects from simply memorizing the reference signal. For Task II the subject is allowed breaks between trials, if necessary. The duration of one entire experiment is 20-25 minutes

Here follows the instructions given to the subjects for the experiments. For the familiarization period the subject is instructed to develop a mapping between their button-press, the color bar for visual feedback, and the beeping speed of the auditory signal. They are also told that in the following task (Task I), the auditory signal will change on its own and they will need to match their button-press to this signal. Before the start of Task II, the subject is linked to the robot and is given a more in-depth explanation on the visual interface, i.e., the reference shoulder trajectory and how the displayed shoulder state depends on their movement. They are then told that the robot will guide their shoulder through the shown trajectory, but not perfectly, and that they will have to correct these errors through slight adjustment, while simultaneously doing the same signal tracking as in the previous Task I. They are also instructed to keep still and only move their shoulder. The subjects are never shown the reference discomfort maps or their own during the experiment, only afterwards will they be made aware that they were trying to recreate a reference map.

For safety reasons, the robot controller gains $\boldsymbol{K}$ and $\boldsymbol{P}_N$ are tuned such that the robot can move the subject's arm, while ensuring that the subject can still easily overpower it. Furthermore, we carefully supervised the subjects, with the robot's emergency stop button at hand.

E. Results

Here, we present and assess the outcomes of the human factors experiments. We begin with a qualitative evaluation, followed by a more quantitative analysis.

For the qualitative evaluation of the results, the difference of the average subject created discomfort maps and subject commanded intensities with the references is analysed. This comparison is shown in Figs. D.1 and E.1 in the appendix. Abridged versions of these figures are shown in Figs. 9 and 10, where the results for references A1 and D can be considered representative for Task I and Task II respectively.

Fig. 10 clearly shows that the subjects lag behind the reference signal. The consequence of this lag is clearly visible in Fig. 9, where the subjects' map for A1 is similar to the reference but rotated clockwise, along the reference trajectory. A similar pattern exists for the other references (see Fig. D.1). Aside from this lag however, the average shape of the discomfort maps is quite similar to the reference.

To estimate the lag the subject commanded intensity is time-shifted relative to the reference intensity. The time-shift where

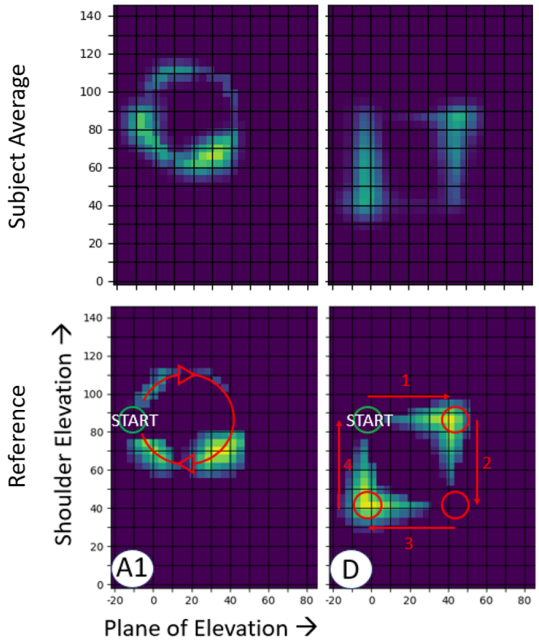

Fig. 9: The average discomfort maps created by the subjects on the top row and the reference maps on the bottom row, for references A1 and D. The overview for all references is shown in Fig. D.1.

TABLE II: Average lag for each reference.

Reference	A1	A2	B	C	D
Average Lag (s)	1.50	1.79	1.15	1.30	1.31
Std. dev. (s)	0.338	0.414	0.576	0.568	0.592

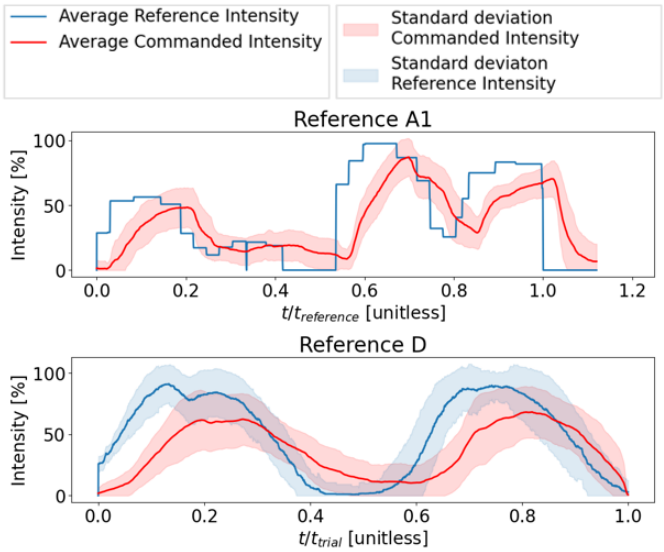

Fig. 10: Plots of the average discomfort intensity commanded by the subjects and the average reference intensity over normalized time for references A1 and D. For reference A1 the reference intensity is the same for all trials, so the time is normalized with the duration of the reference. For D, the reference intensity is different for every trial and every trial has a different duration, because the subjects' shoulder movement is not consistent. So instead the data is normalized with the duration of the trial, then averaged. This is why there is variability in the reference intensity as well. The overview for all references is shown in Fig. E.1.

the error between them is minimal is the lag. The average estimated lag for each reference is shown in Table II. This is approximately 1.4 seconds, which is quite large. The average lag is smallest for B and largest for A2 and A1. The lag for C and D are the same and are intermediate. So the average lag for Task I is larger than for Task II, which is surprising, since the subject has to juggle two assignments at once in the latter. However, the variance in the data is too large to conclude anything statistically significant. Besides the lag, the figures also show, that the subjects' commanded intensity is generally lower than the reference intensity, especially for Task II. This means the subjects are more conservative with their button-press in these trials.

For the quantitative analysis of the results two metrics are designed:

- the map score, which describes how well the subject's drawn discomfort map matches the reference map;
- the intensity score, which describes how well the subject's commanded intensity matches the reference intensity.

The scores are computed as

$$\text{score} = 1 - \frac{\text{RMSE(subject, reference)}}{\text{RMSE(baseline, reference)}}, \tag{9}$$

so the score is the root-mean-square-error (RMSE) between the subject and the reference compared to the RMSE between a baseline and the reference. For the map score, the subject error is defined as the RMSE between their drawn map and the reference map. The baseline error is the RMSE between the reference map and a baseline map, in this case a blank map. For the intensity score, the subject error is the RMSE between the intensity signal created by the subject and the reference signal. The baseline error is the RMSE between the reference signal and a baseline signal of zero. A score of 0 means that the intensity signal or drawn map is as good as the baseline of zero. A score of, for instance, 0.5 means it is 50% better than the baseline and a score of -0.5 means it is 50% worse.

The average scores are shown in Table III and in more detail in Table C.1 in the appendix. From these tables[2] it can be seen that for references A1 and A2 performance is about equal. The scores for C and D are also about equal, which coincides with the average lags. Performance for reference B is the best out of all references, which makes sense as it is the simplest trajectory. This also coincides with B having the lowest average lag. This difference between references is more pronounced in the map scores, which are quite low for C and D.

All scores are greater than 0, meaning the subjects perform better than the baseline. However, the intensity scores hover around 0.4 and the map scores around 0.2, excluding the

[2]For Task I, map scores are omitted. Normally the map scores would also contain information about the subject's shoulder movement, but for Task I the exact same simulated movement is used for every trial. Since no new information is obtained, these map scores are redundant.

scores for B which are especially high. This would mean that for the intensity the subjects perform around 40% above baseline and for the maps only 20%. This is quite low and does not represent our understanding of the results from the qualitative analysis. This discrepancy is most likely caused by the significant lag between the subjects and the reference. This has a more pronounced effect on the discomfort maps, affecting the map scores more than the intensity scores.

TABLE III: Average intensity and map scores.

	Intensity Score					Map Score		
Reference	A1	A2	B	C	D	B	C	D
Min	0.343	0.353	0.330	0.313	0.271	0.117	0.086	0.058
Max	0.482	0.495	0.698	0.516	0.538	0.643	0.333	0.299
Average	0.415	0.420	0.558	0.400	0.408	0.427	0.189	0.192
Std. dev.	0.043	0.047	0.115	0.059	0.097	0.166	0.093	0.082

IV. Discussion

There are several key benefits to the presented approach. It enables patients to quickly and accurately convey points of discomfort and their intensity to the physiotherapist, surpassing the speed of verbal communication and the precision of body language. Furthermore, the push-button interface for discomfort input presented here improves upon similar devices from the studies in [19]–[22] by being single-handed, precise, and not requiring personalization. Moreover, when integrated with a patient movement tracking system, it becomes possible to map their discomfort distribution based on the patient's pose. Though this study only addresses shoulder physiotherapy with a collaborative robot arm, this method could easily be adapted to other parts of the body or different types of robots, like exoskeletons.

Revisiting the topic of strain maps [13], [14]: the strain maps are personalized to the patient and the severity of their injury, however discomfort maps allow for further personalization that even accurate biomechanical models cannot provide. For instance, the discomfort maps also consider sources of discomfort unrelated to rotator cuff tendon strain, such as inflammation in the shoulder, and can take sensitivity to muscle strains into account. Furthermore, as therapy progresses and the patient is able to move in a greater RoM without pain, this change can easily be captured by the discomfort maps. In this way discomfort maps can show progress in the therapy and allow adjustment to the strain maps based on this.

The human factors experiments identified important insights for the practical use of the proposed method. This is the significant time delay between the subject and the discomfort-emulating reference beeping signal of around 1.4 seconds (see Fig. 10 and Table II). This is most likely due to the subject first having to recognize whether the beeping speed has changed and by how much, then calculating how much they should press the push-button based on this. Using frequency modulation for the reference auditory signal instead, would allow for faster detection of changes, thus smaller delay. Nevertheless, the delay would most likely be significantly lower, when the subject reacts to actual discomfort and optimisations can be done to the setup to further reduce the delay, but completely eliminating it is physically impossible. As a consequence, at the time of indicating a discomfort point, the patient will have already moved past this point, so discomfort points in the discomfort maps will be drawn further along the patient's trajectory than they should.

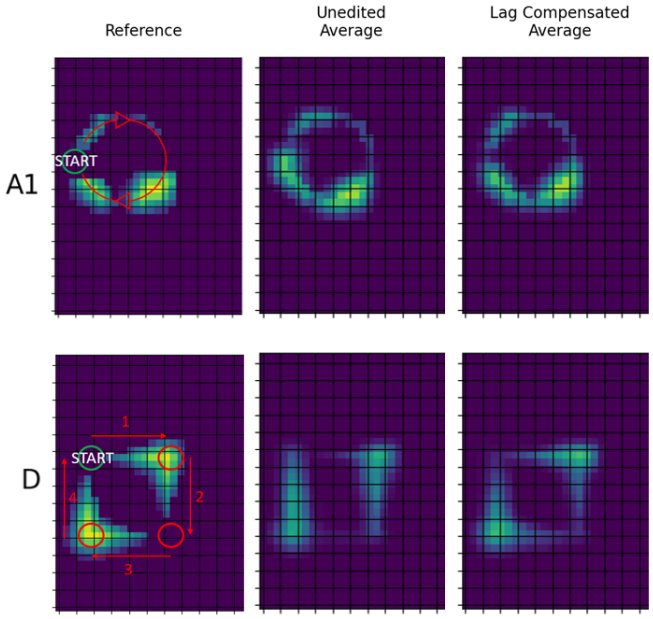

Fig. 11: The average discomfort maps created by the subjects for references A1 and D. The lag-compensated maps are formed by recreating the discomfort map with the same shoulder trajectory, but the commanded intensity is shifted back in time with the estimated time delay for each trial. These maps are then averaged. See Fig. F.1 for all references.

This means that the discomfort maps have the compensate for this delay to be accurate. This can be done by shifting indicated discomfort points back along the patient's trajectory with the delay, either during operation or in post-processing for the next session. An effect of this delay compensation is shown for references A1 and D in Fig. 11, and for all references in Fig. F.1 in the appendix. The lag could result in a situation where at the time of indicating a discomfort point, the patient will have already moved to a more uncomfortable pose, before the robotic system or physiotherapist can react. This problem can be minimized by restricting the movement speed of the robot during the therapy.

It was observed that the best-performing subject, subject 5 (see Table C.1), took more time during the familiarization step of Task I. As such, a longer familiarization period, as well as allowing for periodic re-familiarization throughout the experiments, could improve the overall accuracy. Other factors contributing to differences in scores between subjects, excluding individual responsiveness, may include age, sex, and handedness: Age is associated with an increase in reaction time, although this difference should be negligible within the studied age range of 20-30 [34]. Sex has also been shown to be associated with reaction time; men generally have shorter reaction times than women [35]. However, this trend is not

reflected in the results, as the second-best-performing subject (subject 2) was female, and the performance of the other female participant (subject 7) was intermediate. Handedness could have effected subject performance as well. During the experiments, the left elbow was linked to the robot, while the right hand operated the push-button interface. Right-handed subjects may exhibit greater dexterity in operating the push-button interface, potentially leading to higher intensity and map scores. On the other hand, left-handed subjects might demonstrate greater precision in following the reference shoulder trajectory, which would only contribute to higher map scores. Since information about the subjects' handedness was not documented, no conclusive statements can be made about its influence on the results.

Future work should focus on validating the method for all shoulder DoF, so AR as well, and testing performance when actual discomfort is involved, rather than a quantitative representation of it. If the delay between experiencing discomfort and inputting it remains substantial, practical strategies for implementing the suggested lag compensation should be explored. Additionally, the combination of strain maps and discomfort maps should be further studied.

V. Conclusion

We present a robotic physiotherapy system enabling patients to input poses and their level of discomfort in real-time, generating discomfort maps. These maps represent the patient's discomfort distribution throughout the range of motion, interpretable by both physiotherapists and robots. Through human factors experiments, we have demonstrated the viability of our method during patient-robot interaction. The results also highlight the presence of time delay between the patient feeling and inputting discomfort, and its effect on the generated discomfort maps.

References

[1] "Kuka lbr iiwa." https://www.kuka.com/en-be/products/robotics-systems/industrial-robots/lbr-iiwa. Accessed: 25 October 2023.

[2] H. Minagawa, N. Yamamoto, H. Abe, M. Fukuda, N. Seki, K. Kikuchi, H. Kijima, and E. Itoi, "Prevalence of symptomatic and asymptomatic rotator cuff tears in the general population: From mass-screening in one village," *Journal of Orthopaedics*, vol. 10, pp. 8–12, Mar. 2013.

[3] T. Proietti, V. Crocher, A. Roby-Brami, and N. Jarrasse, "Upper-Limb Robotic Exoskeletons for Neurorehabilitation: A Review on Control Strategies," *IEEE reviews in biomedical engineering*, vol. 9, pp. 4–14, 2016.

[4] H. Østerås and T. A. Torstensen, "The Dose-Response Effect of Medical Exercise Therapy on Impairment in Patients with Unilateral Longstanding Subacromial Pain," *The Open Orthopaedics Journal*, vol. 4, pp. 1–6, Jan. 2010.

[5] "Ticking timebomb: Without immediate action, health and care workforce gaps in the European Region could spell disaster," *World Health Organization*, Sept. 2022.

[6] M. Alexander, "Chapter 1 - Introduction," in *Telerehabilitation* (M. Alexander, ed.), pp. 1–3, New Delhi: Elsevier, Jan. 2022.

[7] D. Simonetti, L. Zollo, E. Papaleo, G. Carpino, and E. Guglielmelli, "Multimodal adaptive interfaces for 3D robot-mediated upper limb neuro-rehabilitation: An overview of bio-cooperative systems," *Robotics and Autonomous Systems*, vol. 85, pp. 62–72, Nov. 2016.

[8] F. Scotto di Luzio, D. Simonetti, F. Cordella, S. Miccinilli, S. Sterzi, F. Draicchio, and L. Zollo, "Bio-Cooperative Approach for the Human-in-the-Loop Control of an End-Effector Rehabilitation Robot," *Frontiers in Neurorobotics*, vol. 12, 2018.

[9] W. Kim, J. Lee, L. Peternel, N. Tsagarakis, and A. Ajoudani, "Anticipatory Robot Assistance for the Prevention of Human Static Joint Overloading in Human-Robot Collaboration," *IEEE Robotics and Automation Letters*, vol. PP, pp. 1–1, July 2017.

[10] L. Peternel, C. Fang, N. Tsagarakis, and A. Ajoudani, "A selective muscle fatigue management approach to ergonomic human-robot co-manipulation," *Robotics and Computer-Integrated Manufacturing*, vol. 58, pp. 69–79, Aug. 2019.

[11] L. F. C. Figueredo, R. C. Aguiar, L. Chen, S. Chakrabarty, M. R. Dogar, and A. G. Cohn, "Human Comfortability: Integrating Ergonomics and Muscular-Informed Metrics for Manipulability Analysis During Human-Robot Collaboration," *IEEE Robotics and Automation Letters*, vol. 6, pp. 351–358, Apr. 2021.

[12] T. Petrič, L. Peternel, J. Morimoto, and J. Babič, "Assistive arm-exoskeleton control based on human muscular manipulability," *Frontiers in Neurorobotics*, vol. 13, 2019.

[13] J. Prendergast, S. Balvert, T. Driessen, A. Seth, and L. Peternel, "Biomechanics Aware Collaborative Robot System for Delivery of Safe Physical Therapy in Shoulder Rehabilitation," *IEEE Robotics and Automation Letters*, vol. 6, no. 4, pp. 7177–7184, 2021.

[14] S. Balvert, M. Prendergast, I. Belli, A. Seth, and L. Peternel, "Enabling Patient- and Teleoperator-led Robotic Physiotherapy via Strain Map Segmentation and Shared-authority," Nov. 2022.

[15] R. B. Fillingim, "Individual differences in pain: understanding the mosaic that makes pain personal," *PAIN*, vol. 158, p. S11, Apr. 2017.

[16] R. Cowen, M. K. Stasiowska, H. Laycock, and C. Bantel, "Assessing pain objectively: the use of physiological markers," *Anaesthesia*, vol. 70, pp. 828–847, July 2015. Publisher: John Wiley & Sons, Ltd.

[17] G. D. De Sario, C. R. Haider, K. C. Maita, R. A. Torres-Guzman, O. S. Emam, F. R. Avila, J. P. Garcia, S. Borna, C. J. McLeod, C. J. Bruce, R. E. Carter, and A. J. Forte, "Using AI to Detect Pain through Facial Expressions: A Review," *Bioengineering*, vol. 10, p. 548, May 2023.

[18] I. S. K. Thong, M. P. Jensen, J. Miró, and G. Tan, "The validity of pain intensity measures: what do the NRS, VAS, VRS, and FPS-R measure?," *Scandinavian Journal of Pain*, vol. 18, pp. 99–107, Jan. 2018. Publisher: De Gruyter.

[19] E. M. Boormans, P. J. Van Kesteren, R. S. Perez, H. A. Brölmann, and W. W. Zuurmond, "Reliability of a Continuous Pain Score Meter: Real Time Pain Measurement," *Pain Practice*, vol. 9, no. 2, pp. 100–104, 2009. _eprint: https://onlinelibrary.wiley.com/doi/pdf/10.1111/j.1533-2500.2009.00260.x.

[20] A. van Wijk, F. Lobbezoo, and J. Hoogstraten, "Reliability and validity of a continuous pain registration procedure," *European Journal of Pain*, vol. 17, no. 3, pp. 394–401, 2013. _eprint: https://onlinelibrary.wiley.com/doi/pdf/10.1002/j.1532-2149.2012.00194.x.

[21] N. Schaffner, G. Folkers, S. Käppeli, M. Musholt, G. F. L. Hofbauer, and V. Candia, "A New Tool for Real-Time Pain Assessment in Experimental and Clinical Environments," *PLoS ONE*, vol. 7, p. e51014, Nov. 2012.

[22] D. M. Böing-Meßing, F. Tomschi, T. Cegla, and T. Hilberg, "The eEgg: Evaluation of a New Device to Measure Pain," *Frontiers in Physiology*, vol. 13, 2022.

[23] L. Peternel, T. Petrič, and J. Babič, "Robotic assembly solution by human-in-the-loop teaching method based on real-time stiffness modulation," *Autonomous Robots*, vol. 42, no. 1, pp. 1–17, 2018.

[24] N. Hogan, "Impedance control - an approach to manipulation. I theory. II - implementation. III - applications," *ASME Transactions Journal of Dynamic Systems and Measurement Control B*, vol. 107, pp. 1–24, 1985.

[25] A. Albu-Schaffer, C. Ott, U. Frese, and G. Hirzinger, "Cartesian impedance control of redundant robots: recent results with the DLR-light-weight-arms," in *2003 IEEE International Conference on Robotics and Automation (Cat. No.03CH37422)*, vol. 3, pp. 3704–3709 vol.3, Sept. 2003. ISSN: 1050-4729.

[26] C. C. De Wit, B. Siciliano, and G. Bastin, eds., *Theory of Robot Control*. Communications and Control Engineering, London: Springer, 1996.

[27] F. Galton, "On instruments for (1) testing perception of differences of tint and for (2) determining reaction time," *Journal of the Anthropological Institute*, vol. 19, pp. 27–29, 1899.

[28] A. T. Welford, "Choice reaction time: Basic concepts," in *Reaction Times* (A. T. Welford, ed.), 1980.

[29] J. T. Brebner and A. T. Welford, "Introduction: an historical background sketch," in *Reaction Times* (A. T. Welford, ed.), pp. 1–23, New York: Academic Press, 1980.
[30] E. S. Robinson, "Work of the integrated organism," in *A handbook of general experimental psychology*, pp. 571–650, Worcester: Clark University Press, 1934.
[31] A. F. Sanders, *Elements of human performance: Reaction processes and attention in human skill*. Psychology Press, Jan. 2013.
[32] R. J. Kosinski, "Literature Review on Reaction Time," 2012.
[33] J. Ravenberg, "Functionality Test: Discomfort Map Creation Demo." https://www.youtube.com/watch?v=pzcACqyejdc.
[34] R. Gottsdanker, "Age and simple reaction time," *Journal of Gerontology*, vol. 37, pp. 342–348, May 1982.
[35] A. Jain, R. Bansal, A. Kumar, and K. Singh, "A comparative study of visual and auditory reaction times on the basis of gender and physical activity levels of medical first year students," *International Journal of Applied and Basic Medical Research*, vol. 5, no. 2, p. 124, 2015.

2

Appendix

APPENDIX A
SHOULDER STATE ESTIMATION

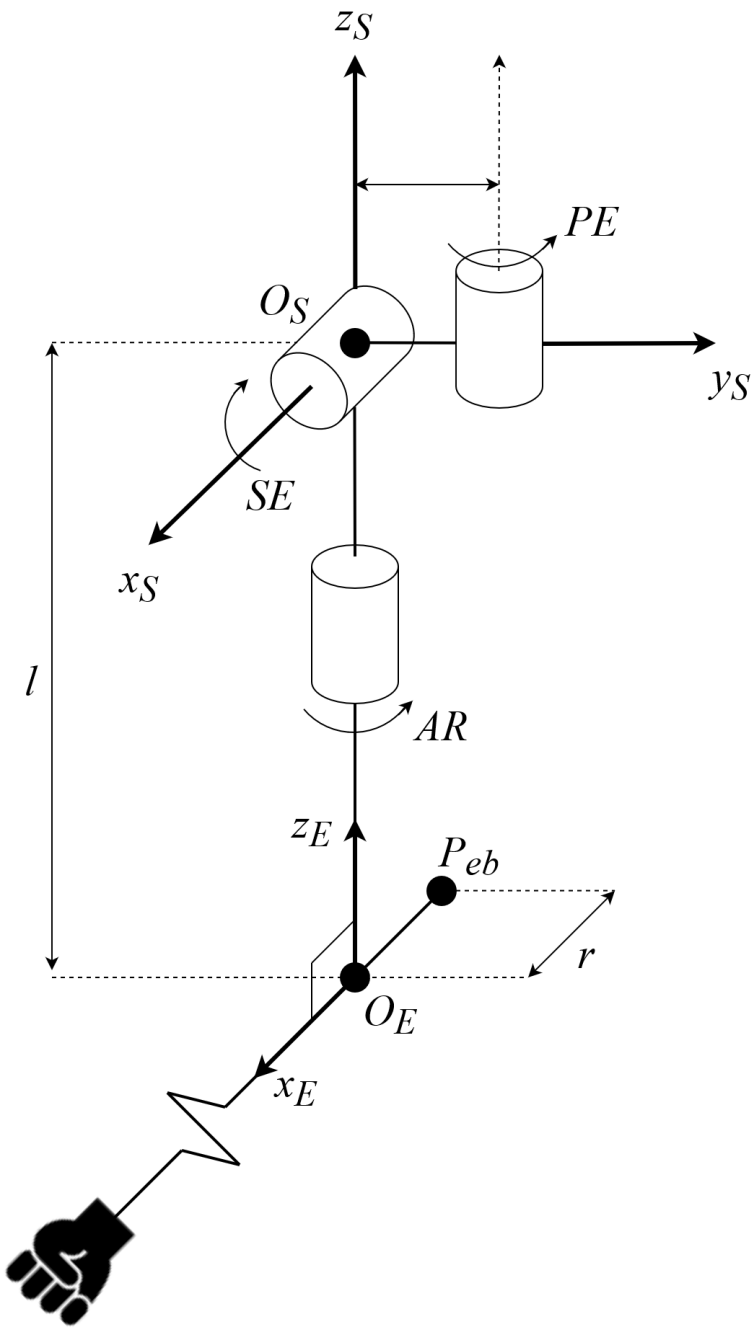

Fig. A.1: Kinematic model of the right arm used for calculating the robot end-effector pose needed to move the shoulder to a commanded state and for estimating the shoulder state from the measured robot end-effector pose. Two frames are drawn: the shoulder frame S with origin $\boldsymbol{O}_S$ and the elbow frame E with origin $\boldsymbol{O}_E$. Also drawn are the DoF of the glenohumeral joint: axial rotation (AR), plane of elevation (PE) and shoulder elevation (SE). The values l and r are the length and radius of the upper arm respectively, $\boldsymbol{P}_{eb}$ is the back of the elbow. The model for the left arm is the same, but mirrored in the $x_S z_S$-plane.

The robot arm holds onto the elbow of the patient with a custom L-shaped brace. This keeps the elbow at a 90° angle, but more importantly aligns the frame of the robot end-effector with that of the patient's elbow, see Fig. 3. This allows the shoulder state of the patient to be estimated from the robot end-effector pose using a simple kinematic model, shown in Fig. A.1.

This model is used to predict the pose of the robot end-effector given a certain shoulder state (forward kinematics) and the reverse, i.e., to estimate the shoulder state from the robot end-effector pose (inverse kinematics). The forward and inverse kinematics allow you to move the patient's arm to a given configuration using the robot, and estimate their state based on the robot position, respectively. The right shoulder is used as reference, using the right-handed convention.

The following frames are considered:

- the world frame W;
- the shoulder frame S: centered at the the right humeral head of the patient with x_S parallel to the sagittal plane and pointing forward, z_S is also parallel to the sagittal plane but points upward. y_S lies in the frontal plane of the patient and points to the left shoulder;
- the elbow frame E: assumes the elbow is locked at a 90° angle, x_E points along the lower arm, and z_E points to the shoulder along the upper arm. In a resting position, i.e., AR = PE = SE = 0, this frame is parallel to the shoulder frame;
- the robot end-effector frame R, which is aligned to the elbow frame E.

A. Forward Kinematics

In order to predict the robot end-effector pose given a shoulder state, the goal is to compute the transformation from the world frame to the robot frame $\boldsymbol{T}_{W\rightarrow R}$ from the transformation of the shoulder frame to the elbow frame $\boldsymbol{T}_{S\rightarrow E}$ when shoulder state $\boldsymbol{\alpha}$ and everything else is known.

The shoulder is modeled as a sequence of three rotational joints; a ZXZ Euler-angle sequence with PE, (-)SE, and AR respectively. $\boldsymbol{T}_{S\rightarrow E}$ is then given by these rotations followed by a translation of $-l$ (length of the upper arm) along the resultant z-axis. From this follows:

$$\boldsymbol{T}_{W\rightarrow R} \equiv \boldsymbol{T}_{W\rightarrow E} = \boldsymbol{T}_{W\rightarrow S} \cdot \boldsymbol{T}_{S\rightarrow E}, \tag{10}$$

with which the robot end-effector pose in the world frame for commanding to the robot can be computed

B. Inverse Kinematics

In order to estimate the shoulder state from the robot end-effector pose, the goal is to find the transformation from the shoulder frame to the elbow frame $\boldsymbol{T}_{S\rightarrow E}$, when $\boldsymbol{\alpha}$ is unknown, but everything else is known. The difference with the forward kinematics is that this transformation cannot be directly computed, however $\boldsymbol{T}_{W\rightarrow E}$ is already known from reading out the robot encoders.

The robot end-effector position $\boldsymbol{P}_{ee}$ in the world frame is first transformed to the shoulder frame. For this, the a priori knowledge that the robot end-effector and the shoulder are kinematically linked by the upper arm of the patient is used: $\boldsymbol{P}_{ee}^{S}$ is first mapped to the closest point on the sphere with radius l centered at the base of the shoulder $\boldsymbol{O}_{S}^{S}$, this point is $\bar{\boldsymbol{P}}_{ee}^{S}$. PE is estimated from the angle between this vector projected unto the x_Sy_S-plane and the -y_S-axis, SE is estimated from the angle between $\bar{\boldsymbol{P}}_{ee}^{S}$ and the z_S axis.

Finally, to calculate AR the measured elbow frame is compared to the elbow frame in the case of AR is zero E_0, which is calculated using the PE and SE calculated above, analogous to the forward kinematics. The rotation between these two frames is of course equal to AR. To analyse this rotation an arbitrary known point on the plane perpendicular to the axis of rotation z_E in the elbow frames has to be studied. Here the back of the elbow is chosen, which is defined as

$$\boldsymbol{P}_{eb}^{E} \equiv [-r\ 0\ 0]^{E}, \tag{11}$$

where r is the upper arm radius. This point is compared to the back of the elbow in case AR is zero:

$$\boldsymbol{P}_{eb0}^{E_0} \equiv [-r\ 0\ 0]^{E_0}. \tag{12}$$

The angle between these two points in (either) elbow frame is AR as it represents the angle between the real elbow frame and the predicted elbow frame when AR=0, under the assumption that these frames have the same origin.

In order to compare these two points, they have to first be expressed in the same frame. As stated before frame E is unknown, i.e., $\boldsymbol{T}_{W\rightarrow E}$ and $\boldsymbol{T}_{S\rightarrow E}$ are unknown. However $\boldsymbol{P}_{eb}^{W}$ is known in the world frame through encoder measurements and $\boldsymbol{T}_{S\rightarrow E_0}$ was just calculated. $\boldsymbol{P}_{eb}^{W}$ can be transformed to $\boldsymbol{P}_{eb}^{E_0}$ with

$$\boldsymbol{T}_{W\rightarrow E_0} = \boldsymbol{T}_{W\rightarrow S} \cdot \boldsymbol{T}_{S\rightarrow E_0}. \tag{13}$$

AR is then the angle between $\boldsymbol{P}_{eb}^{E_0}$ and $\boldsymbol{P}_{eb0}^{E_0}$.

Derivation of the forward and inverse kinematics is the same for the left shoulder, except everything is mirrored in the x_Sz_S-plane.

APPENDIX B
FUNCTIONALITY TEST AR DEMO

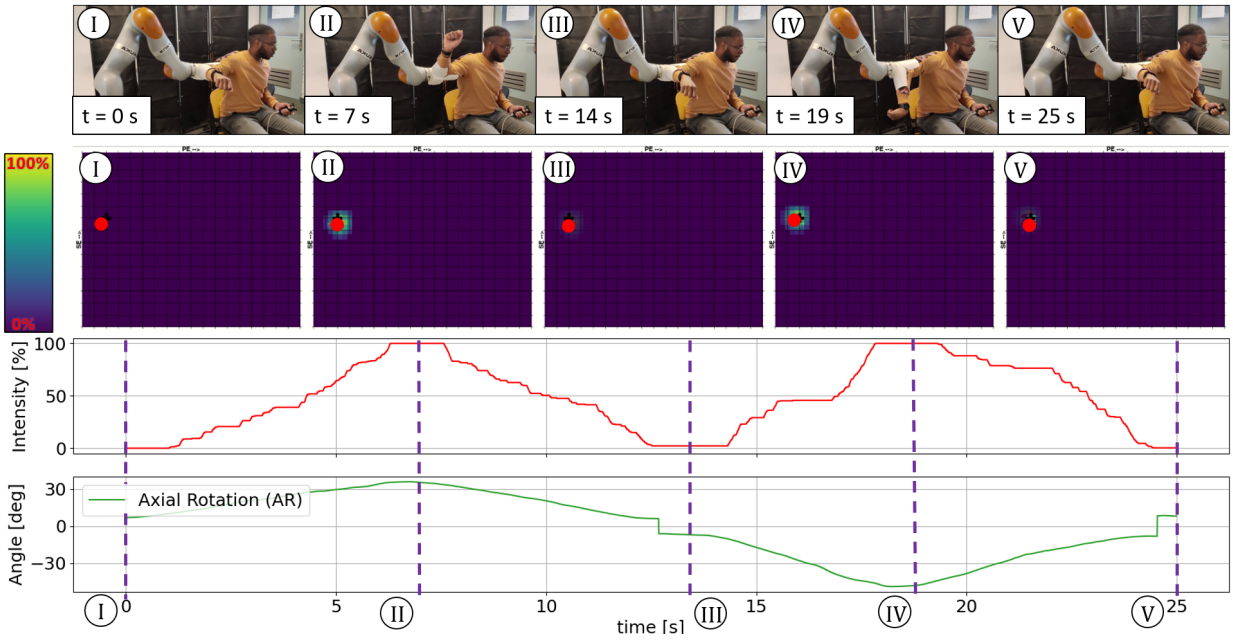

Fig. B.1: Demonstration of discomfort map creation using the proposed method, with snapshots taken at specific timestamps A to E. The first row shows the robot and subject poses at these timestamps. The second row shows the discomfort map at these timestamps, with the current shoulder state marked as a filled red dot. The third row shows the discomfort intensity commanded by the subject over time, i.e., how much the push-button is pressed. The fourth row shows the AR angle over time. PE and SE are missing from this overview for brevity, because they are approximately constant at 0° and 90° respectively. Note: The images in the first row are mirrored for demonstration purposes.

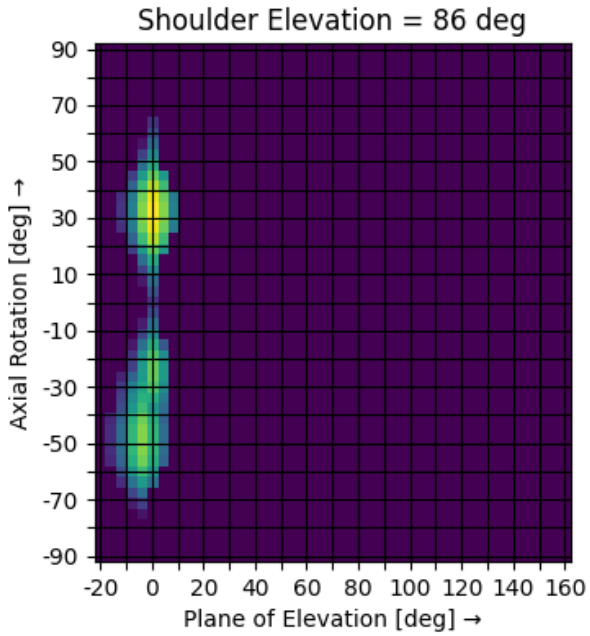

Fig. B.2: PE-AR projection of the discomfort map created from the demonstration in Fig. B.1 at a fixed shoulder elevation of 86°.

APPENDIX C
SUBJECT SCORE OVERVIEW

TABLE C.1: Average intensity and map scores for every subject.

	Intensity Score					Map Score		
Reference	A1	A2	B	C	D	B	C	D
Subject 1	0.375	0.402	0.411	0.357	0.377	0.414	0.224	0.249
Subject 2	0.482	0.426	0.698	0.449	0.511	0.616	0.243	0.224
Subject 3	0.343	0.379	0.330	0.353	0.271	0.117	0.092	0.058
Subject 4	0.369	0.353	0.634	0.376	0.298	0.380	0.121	0.072
Subject 5	0.463	0.483	0.661	0.516	0.538	0.643	0.253	0.299
Subject 6	0.424	0.441	0.542	0.443	0.402	0.463	0.127	0.230
Subject 7	0.403	0.365	0.534	0.397	0.419	0.251	0.333	0.225
Subject 8	0.446	0.495	0.580	0.313	0.506	0.350	0.102	0.183
Subject 9	0.416	0.412	0.540	0.367	0.292	0.438	0.086	0.120
Subject 10	0.430	0.447	0.646	0.425	0.462	0.595	0.305	0.260
Min	0.343	0.353	0.330	0.313	0.271	0.117	0.086	0.058
Max	0.482	0.495	0.698	0.516	0.538	0.643	0.333	0.299
Average	0.415	0.420	0.558	0.400	0.408	0.427	0.189	0.192
Std. dev.	0.043	0.047	0.115	0.059	0.097	0.166	0.093	0.082

APPENDIX D
AVERAGE SUBJECT DISCOMFORT MAPS

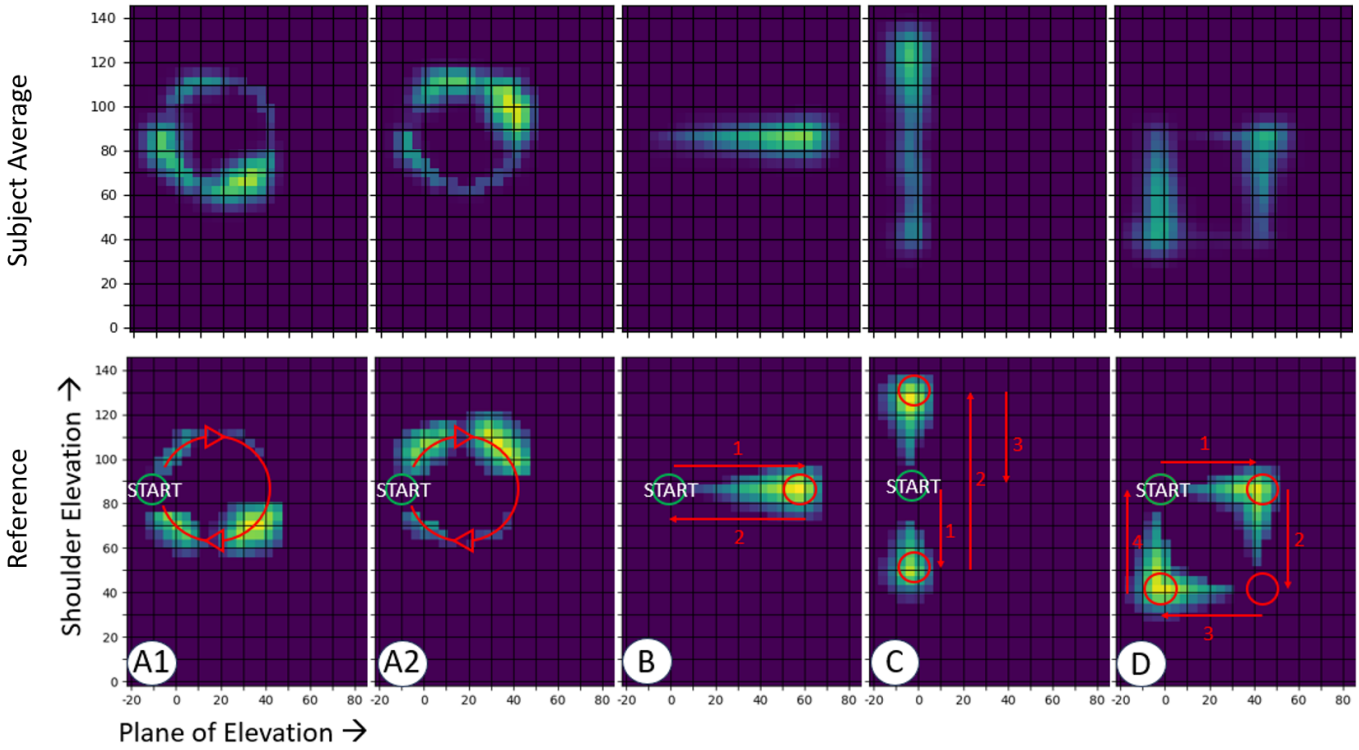

Fig. D.1: The average discomfort maps created by the subjects on the top row and the reference maps on the bottom row.

APPENDIX E
AVERAGE SUBJECT COMMANDED INTENSITY

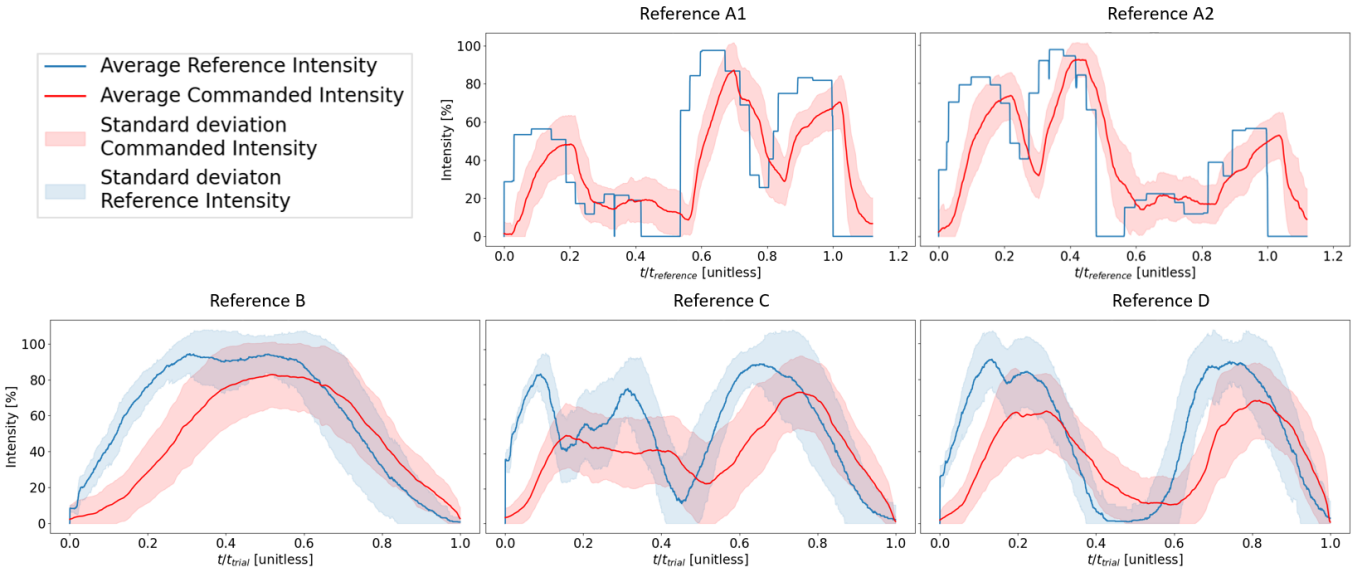

Fig. E.1: Plots of the average discomfort intensity commanded by the subjects and the average reference intensity over normalized time. For references A1 and A2 the reference intensity is the same for all trials, so the time is normalized with the duration of the reference. For B, C and D, the reference intensity is different for every trial and every trial has a different duration, because the subjects' shoulder movement is not consistent. So instead the data is normalized with the duration of the trial, then averaged. This is why there is variability in the reference intensity as well

APPENDIX F
AVERAGE LAG-COMPENSATED SUBJECT DISCOMFORT MAPS

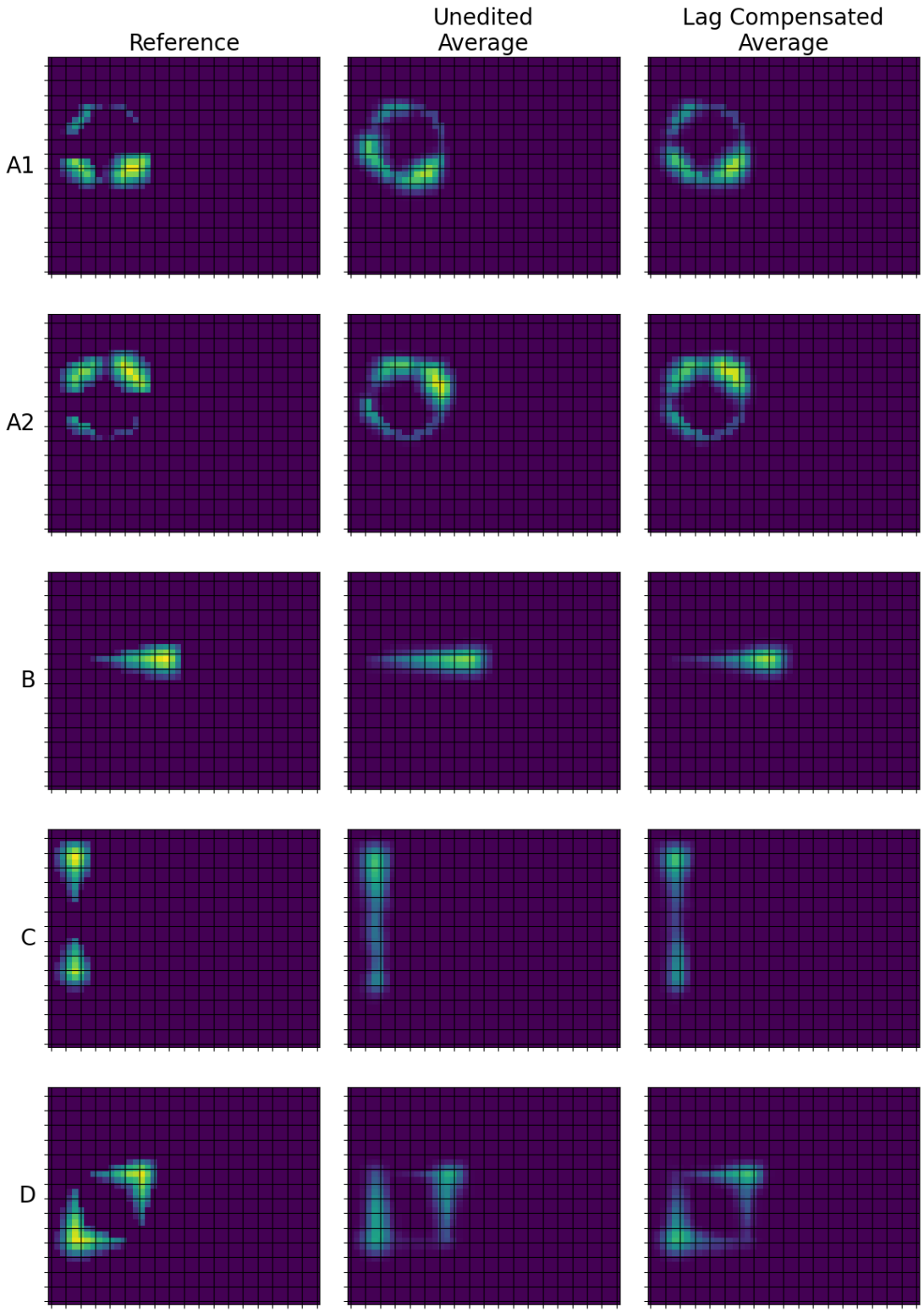

Fig. F.1: The average discomfort maps created by the subjects compensated for time delay. The lag-compensated maps are formed by recreating the discomfort map with the same shoulder trajectory, but the commanded intensity is shifted back in time with the estimated time delay for each trial. These maps are then averaged.

APPENDIX G
DETAILED RESULTS PER SUBJECT

Starting from the following page, an overview of the results for the human factors experiments for all 10 subjects is shown. This includes the drawn discomfort map, the subject commanded intensity and reference intensity (from 0% to 100%) over time, and the intensity and map scores for all trials. For illustration, the reference maps are also shown and accompanied by a "perfect example", which shows the reference intensity when the reference trajectory is followed perfectly. However, references A1 and A2 do not show a perfect example, because the shoulder movement is then simulated by the reference trajectory, thus the reference intensity is already "perfect".

A. *Subject 1*

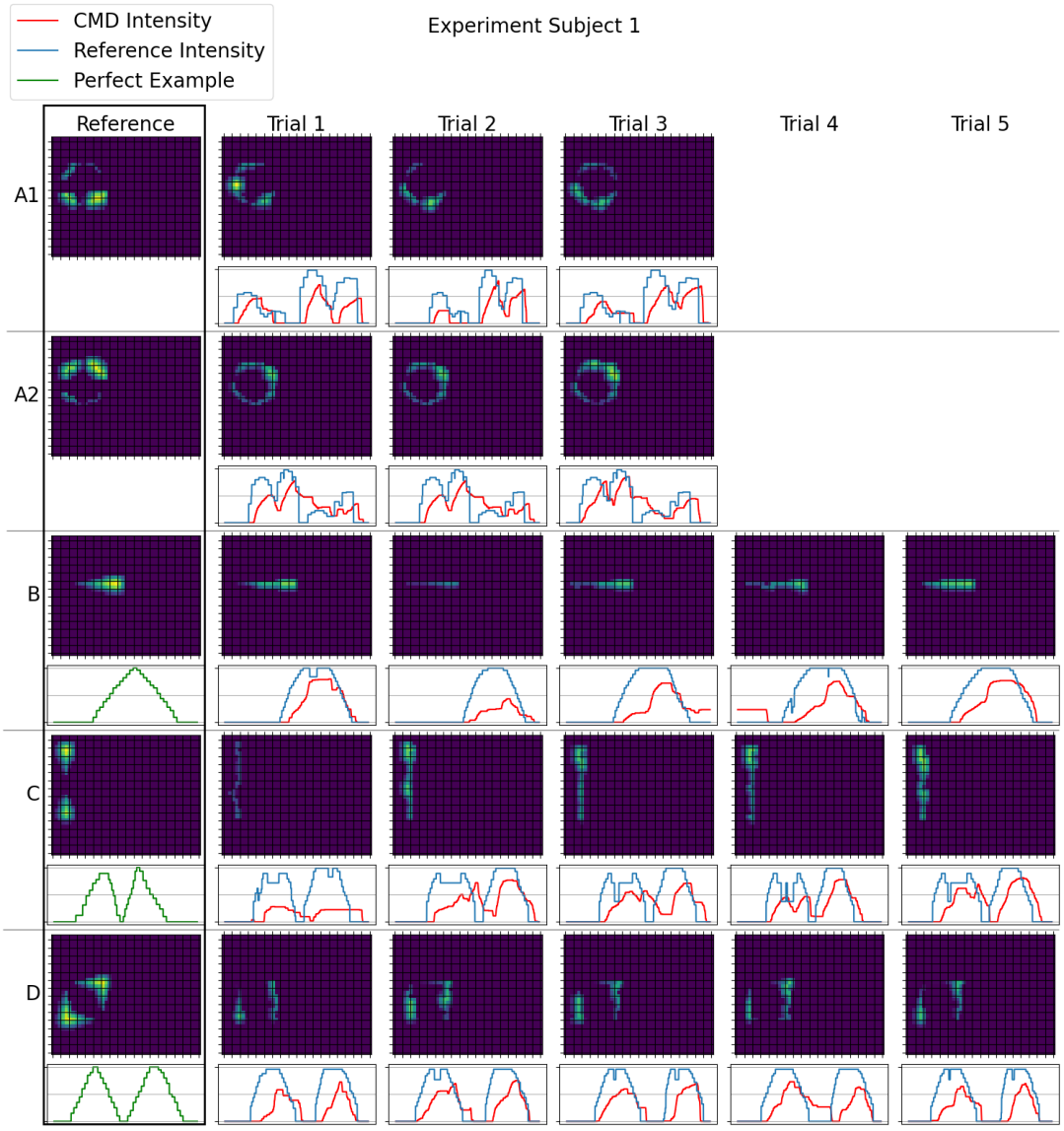

Fig. G.1: Discomfort maps and plots of reference intensity vs subject commanded intensity over time for subject 1.

TABLE G.1: Intensity and map scores for subject 1.

	Intensity					Map		
Reference	A1	A2	B	C	D	B	C	D
Trial 1	0.349	0.386	0.556	0.216	0.3	0.49	0.136	0.192
Trial 2	0.373	0.386	0.267	0.405	0.428	0.164	0.249	0.2
Trial 3	0.403	0.436	0.356	0.351	0.429	0.478	0.262	0.297
Trial 4	-	-	0.357	0.418	0.362	0.438	0.299	0.257
Trial 5	-	-	0.518	0.395	0.369	0.501	0.172	0.297
Min	0.349	0.386	0.267	0.216	0.3	0.164	0.136	0.192
Max	0.403	0.436	0.556	0.418	0.429	0.501	0.299	0.297
Average	0.375	0.402	0.411	0.357	0.377	0.414	0.224	0.249
Std. dev.	0.027	0.029	0.122	0.083	0.054	0.142	0.067	0.051

B. Subject 2

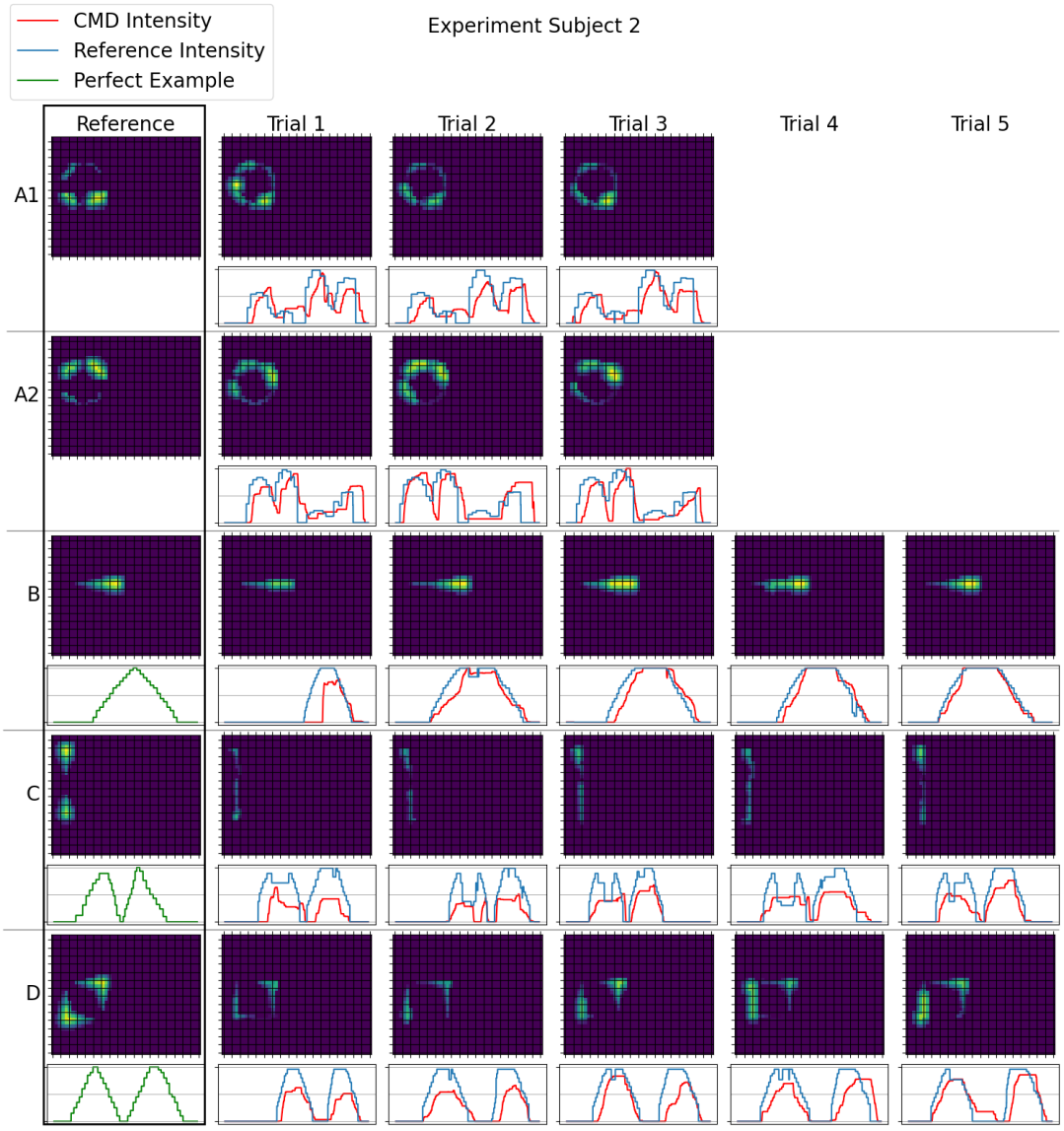

Fig. G.2: Discomfort maps and plots of reference intensity vs subject commanded intensity over time for subject 2.

TABLE G.2: Intensity and map scores for subject 2.

	Intensity					Map		
Reference	A1	A2	B	C	D	B	C	D
Trial 1	0.466	0.41	0.373	0.322	0.49	0.612	0.178	0.262
Trial 2	0.452	0.39	0.734	0.362	0.467	0.488	0.173	0.258
Trial 3	0.528	0.479	0.733	0.513	0.517	0.618	0.274	0.242
Trial 4	-	-	0.778	0.507	0.487	0.622	0.226	0.118
Trial 5	-	-	0.87	0.542	0.593	0.742	0.364	0.24
Min	0.452	0.39	0.373	0.322	0.467	0.488	0.173	0.118
Max	0.528	0.479	0.87	0.542	0.593	0.742	0.364	0.262
Average	0.482	0.426	0.698	0.449	0.511	0.616	0.243	0.224
Std. dev.	0.04	0.047	0.19	0.1	0.049	0.09	0.079	0.06

C. Subject 3

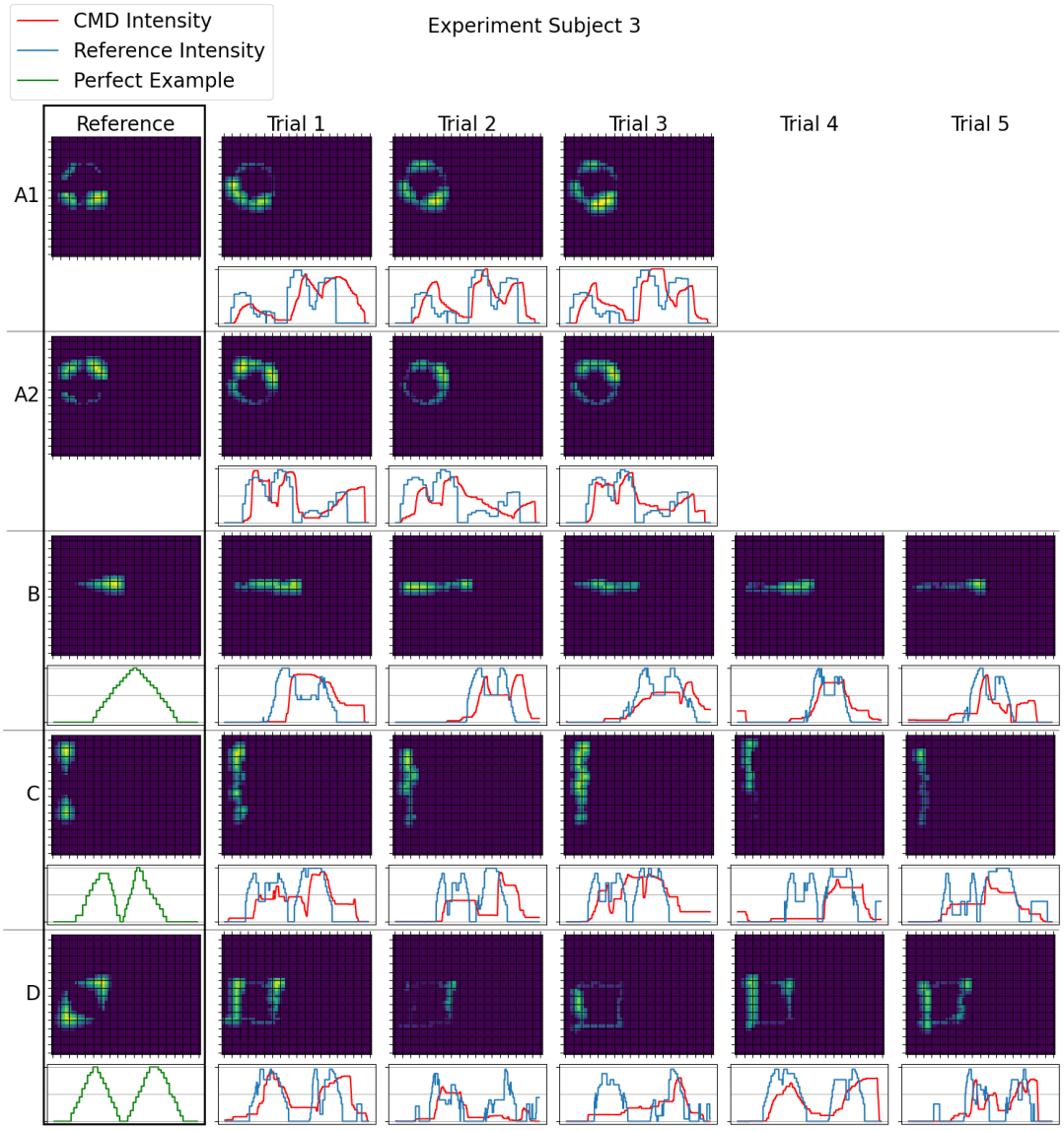

Fig. G.3: Discomfort maps and plots of reference intensity vs subject commanded intensity over time for subject 3.

TABLE G.3: Intensity and map scores for subject 3.

	Intensity					Map		
Reference	A1	A2	B	C	D	B	C	D
Trial 1	0.232	0.316	0.158	0.442	0.342	0.199	0.239	0.118
Trial 2	0.43	0.316	0.2	0.148	0.231	-0.177	-0.005	0.006
Trial 3	0.369	0.505	0.486	0.383	0.253	0.178	-0.109	0.104
Trial 4	-	-	0.507	0.302	0.33	0.261	0.096	0.128
Trial 5	-	-	0.3	0.489	0.2	0.126	0.239	-0.068
Min	0.232	0.316	0.158	0.148	0.2	-0.177	-0.109	-0.068
Max	0.43	0.505	0.507	0.489	0.342	0.261	0.239	0.128
Average	0.343	0.379	0.33	0.353	0.271	0.117	0.092	0.058
Std. dev.	0.101	0.109	0.161	0.134	0.062	0.172	0.152	0.086

D. Subject 4

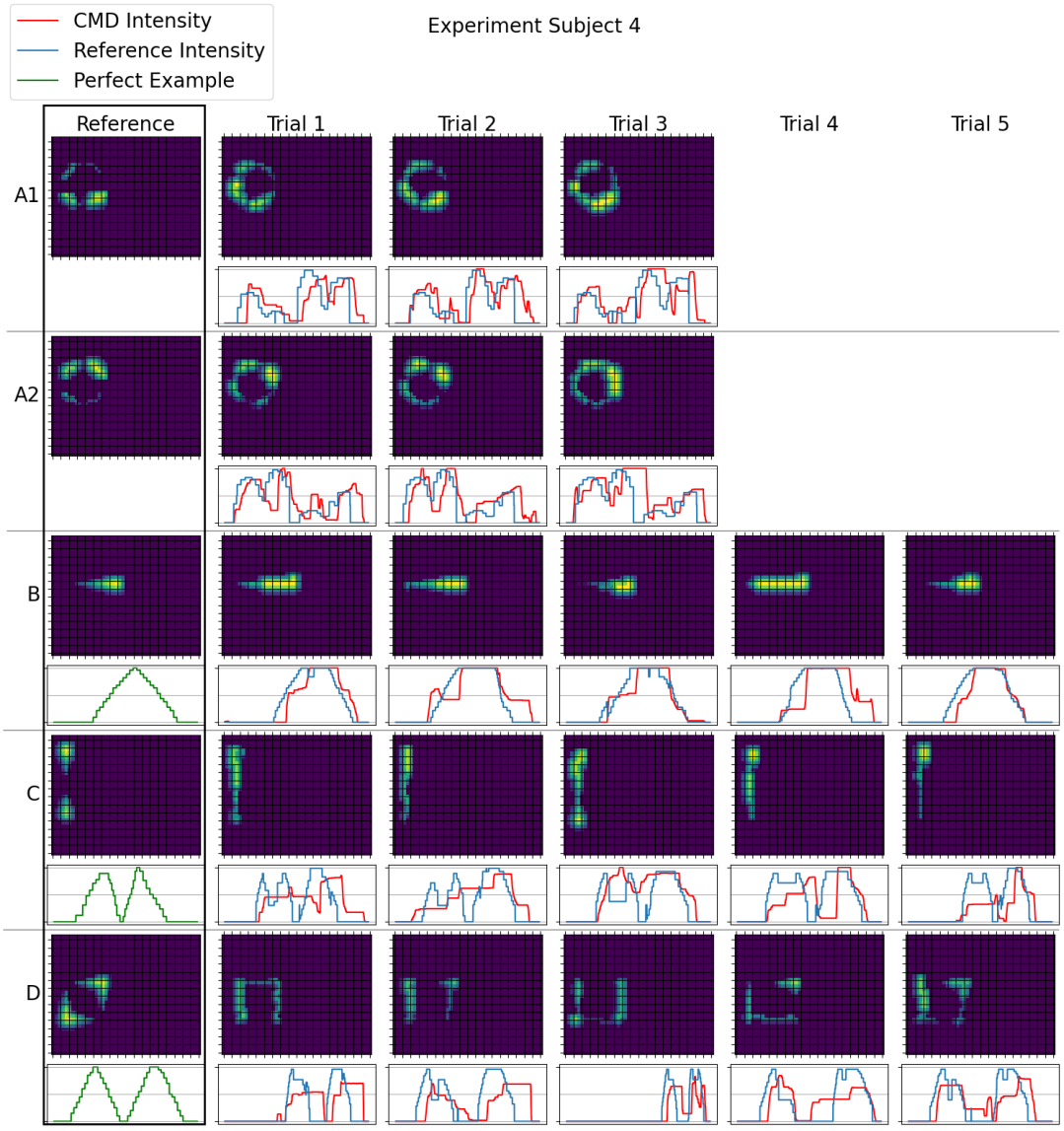

Fig. G.4: Discomfort maps and plots of reference intensity vs subject commanded intensity over time for subject 4.

TABLE G.4: Intensity and map scores for subject 4.

	Intensity					Map		
Reference	A1	A2	B	C	D	B	C	D
Trial 1	0.377	0.366	0.66	0.301	0.195	0.268	0.128	0.091
Trial 2	0.39	0.409	0.608	0.48	0.204	0.491	0.194	0.011
Trial 3	0.341	0.283	0.73	0.395	0.265	0.582	-0.023	0.022
Trial 4	-	-	0.452	0.321	0.419	-0.075	0.051	0.19
Trial 5	-	-	0.719	0.384	0.41	0.636	0.256	0.046
Min	0.341	0.283	0.452	0.301	0.195	-0.075	-0.023	0.011
Max	0.39	0.409	0.73	0.48	0.419	0.636	0.256	0.19
Average	0.369	0.353	0.634	0.376	0.298	0.38	0.121	0.072
Std. dev.	0.025	0.064	0.113	0.071	0.109	0.291	0.111	0.072

E. Subject 5

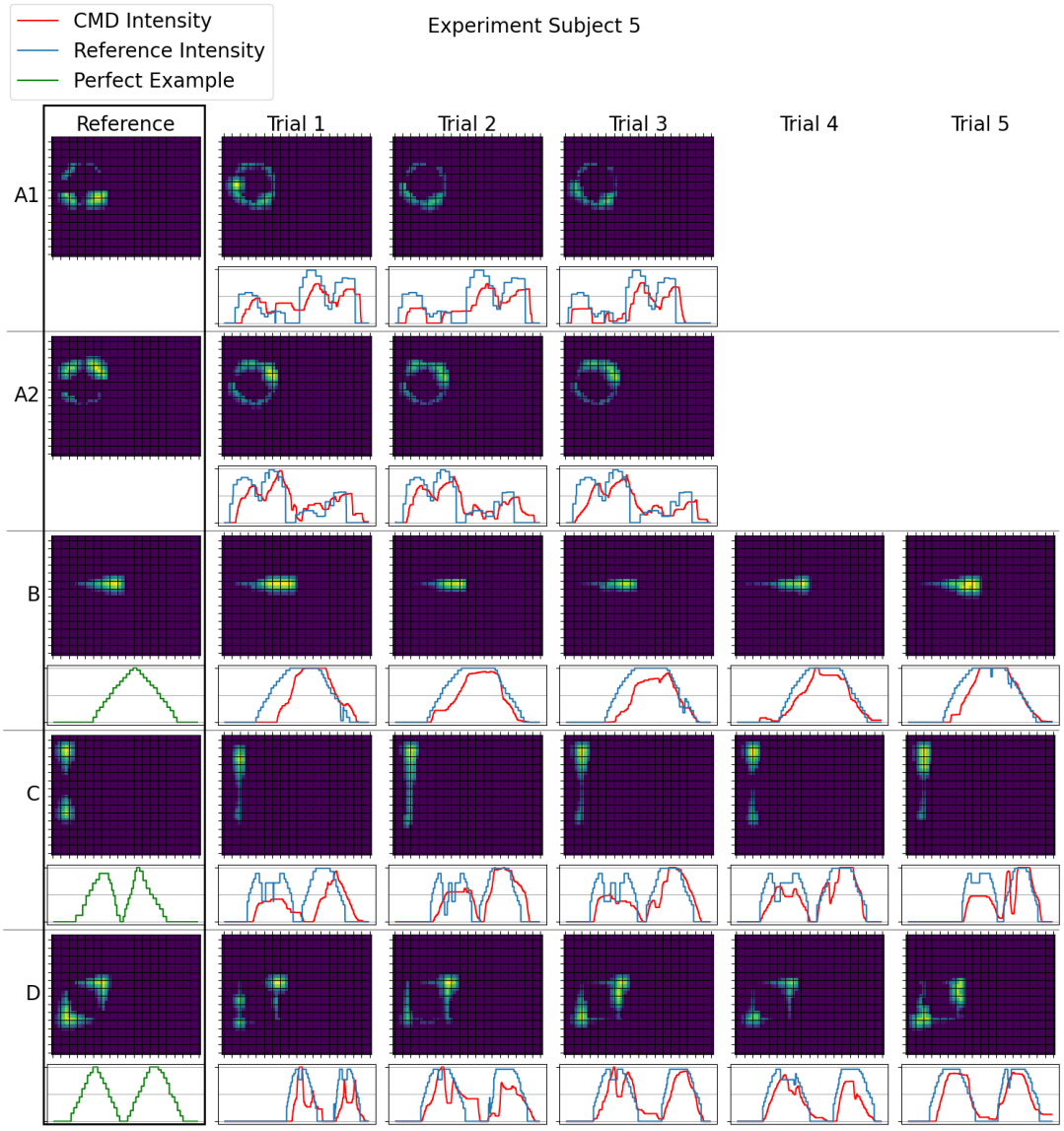

Fig. G.5: Discomfort maps and plots of reference intensity vs subject commanded intensity over time for subject 5.

TABLE G.5: Intensity and map scores for subject 5.

	Intensity					Map		
Reference	A1	A2	B	C	D	B	C	D
Trial 1	0.474	0.463	0.545	0.348	0.391	0.589	0.199	0.169
Trial 2	0.456	0.496	0.687	0.512	0.469	0.688	0.199	0.263
Trial 3	0.458	0.489	0.616	0.553	0.609	0.669	0.296	0.274
Trial 4	-	-	0.76	0.624	0.571	0.671	0.343	0.361
Trial 5	-	-	0.697	0.543	0.651	0.596	0.228	0.429
Min	0.456	0.463	0.545	0.348	0.391	0.589	0.199	0.169
Max	0.474	0.496	0.76	0.624	0.651	0.688	0.343	0.429
Average	0.463	0.483	0.661	0.516	0.538	0.643	0.253	0.299
Std. dev.	0.01	0.018	0.083	0.102	0.106	0.047	0.064	0.099

F. Subject 6

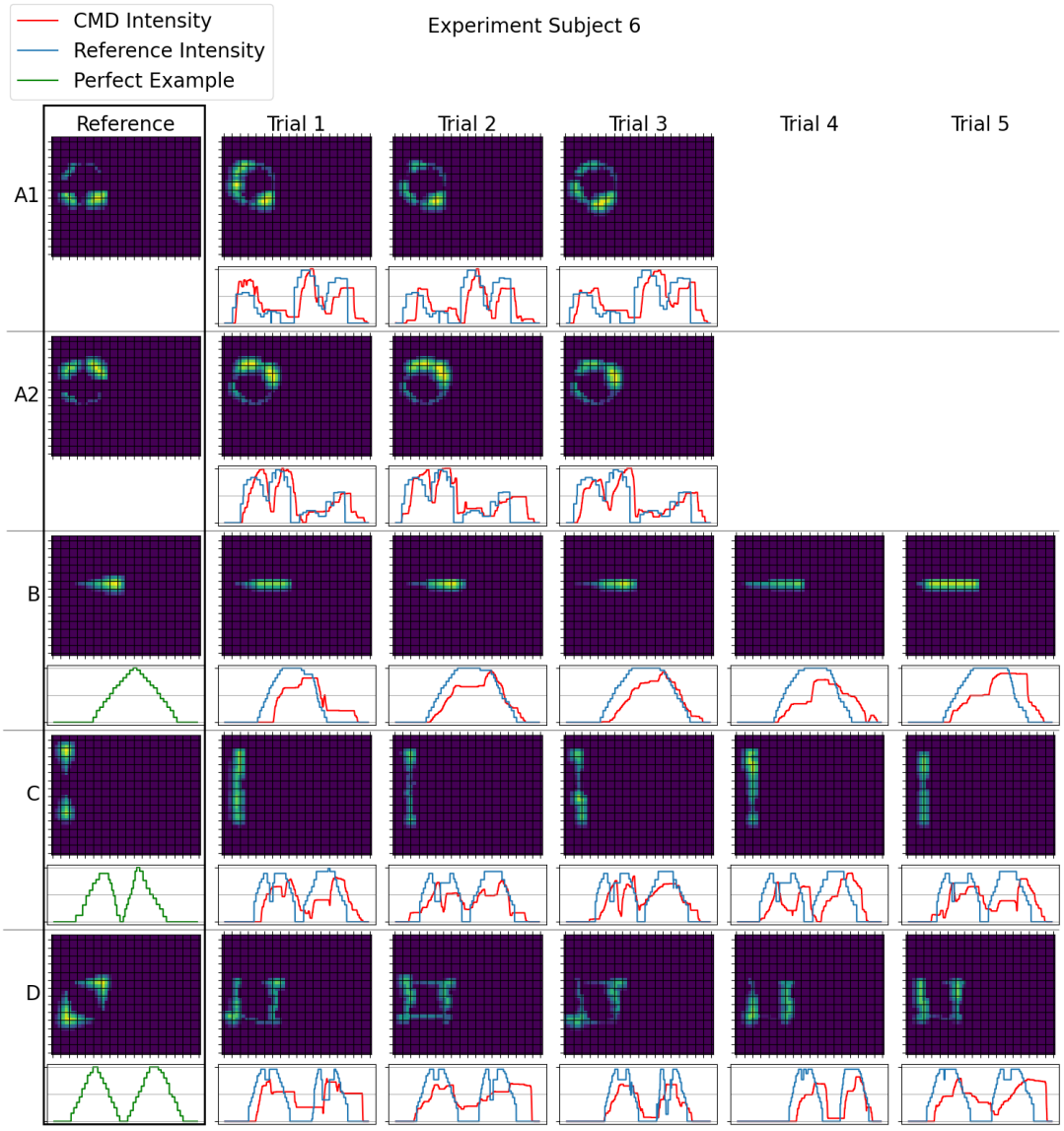

Fig. G.6: Discomfort maps and plots of reference intensity vs subject commanded intensity over time for subject 6.

TABLE G.6: Intensity and map scores for subject 6.

	Intensity					Map		
Reference	A1	A2	B	C	D	B	C	D
Trial 1	0.468	0.447	0.507	0.429	0.367	0.422	0.066	0.252
Trial 2	0.399	0.446	0.657	0.544	0.394	0.605	0.242	0.147
Trial 3	0.406	0.43	0.614	0.546	0.532	0.651	0.26	0.336
Trial 4	-	-	0.467	0.295	0.416	0.459	0.01	0.199
Trial 5	-	-	0.467	0.399	0.301	0.181	0.057	0.214
Min	0.399	0.43	0.467	0.295	0.301	0.181	0.01	0.147
Max	0.468	0.447	0.657	0.546	0.532	0.651	0.26	0.336
Average	0.424	0.441	0.542	0.443	0.402	0.463	0.127	0.23
Std. dev.	0.038	0.009	0.088	0.106	0.084	0.185	0.115	0.07

G. Subject 7

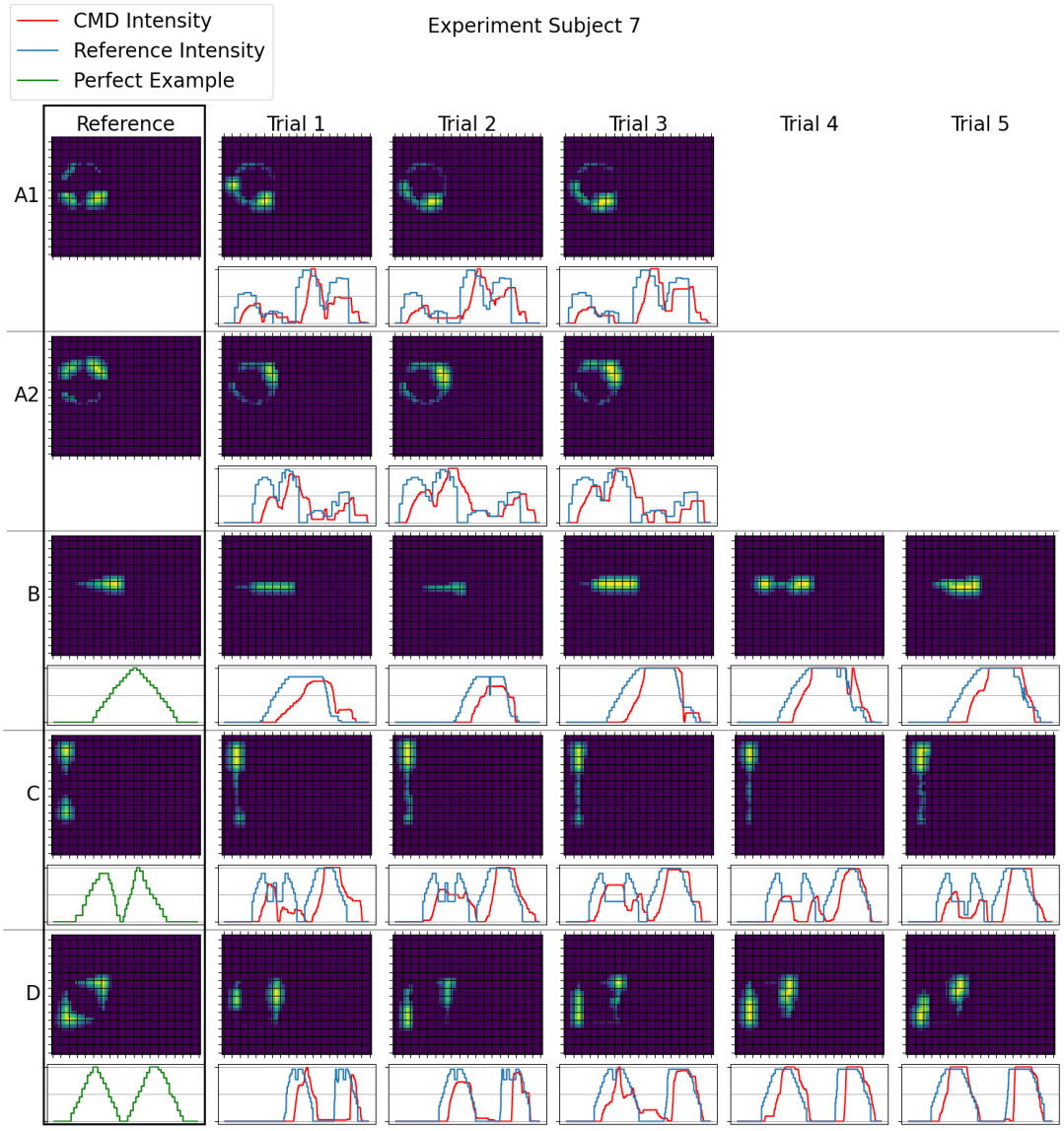

Fig. G.7: Discomfort maps and plots of reference intensity vs subject commanded intensity over time for subject 7.

TABLE G.7: Intensity and map scores for subject 7.

	Intensity					Map		
Reference	A1	A2	B	C	D	B	C	D
Trial 1	0.421	0.346	0.427	0.346	0.187	0.271	0.313	0.002
Trial 2	0.387	0.344	0.47	0.436	0.408	0.229	0.336	0.301
Trial 3	0.401	0.406	0.566	0.425	0.491	0.303	0.346	0.323
Trial 4	-	-	0.607	0.369	0.45	0.097	0.387	0.203
Trial 5	-	-	0.6	0.409	0.561	0.357	0.28	0.296
Min	0.387	0.344	0.427	0.346	0.187	0.097	0.28	0.002
Max	0.421	0.406	0.607	0.436	0.561	0.357	0.387	0.323
Average	0.403	0.365	0.534	0.397	0.419	0.251	0.333	0.225
Std. dev.	0.017	0.035	0.081	0.038	0.142	0.098	0.04	0.133

H. Subject 8

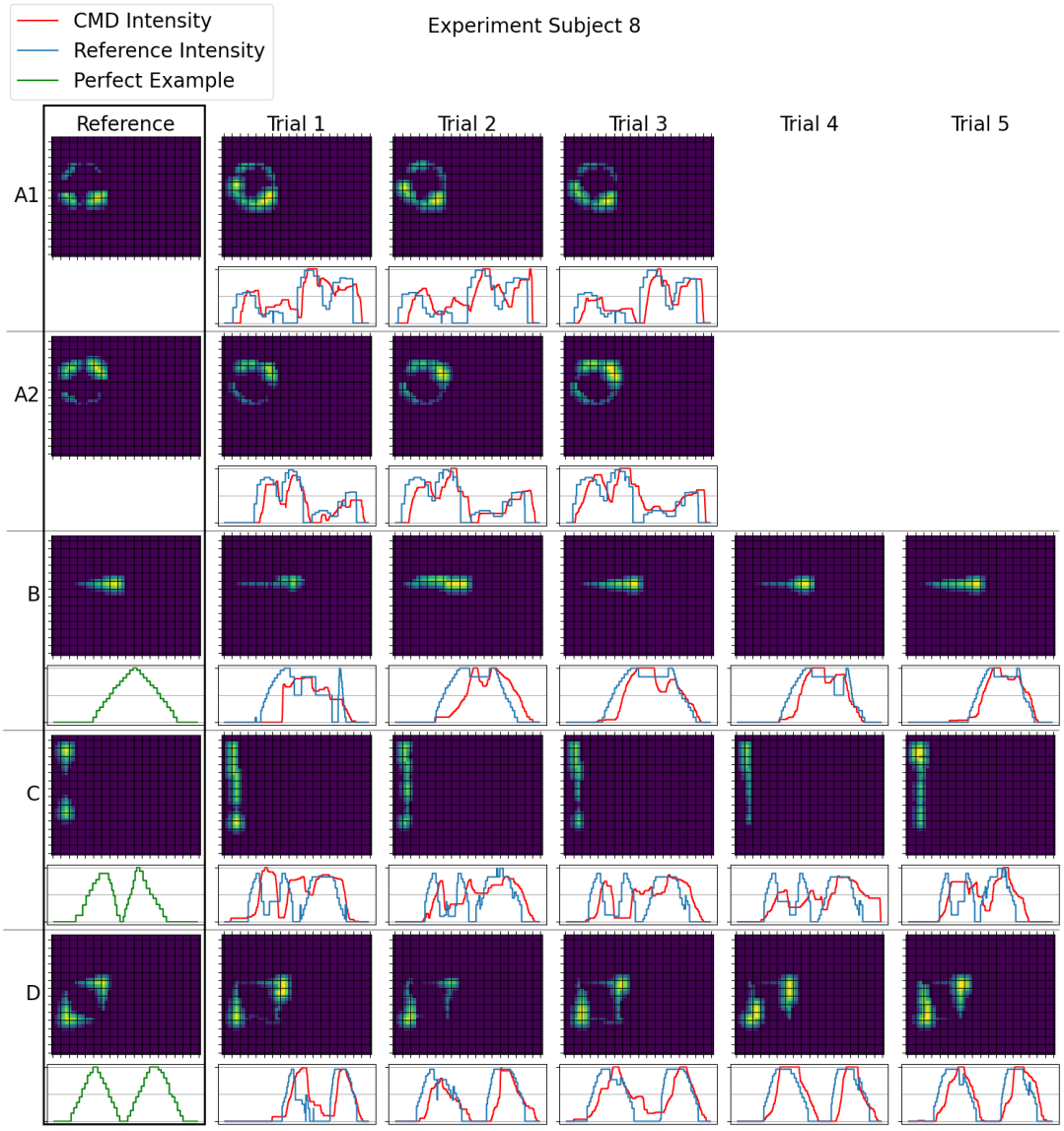

Fig. G.8: Discomfort maps and plots of reference intensity vs subject commanded intensity over time for subject 8.

TABLE G.8: Intensity and map scores for subject 8.

	Intensity					Map		
Reference	A1	A2	B	C	D	B	C	D
Trial 1	0.458	0.519	0.401	0.194	0.385	0.257	-0.136	0.127
Trial 2	0.425	0.482	0.468	0.399	0.512	0.176	0.112	0.256
Trial 3	0.455	0.483	0.671	0.259	0.549	0.497	0.106	0.236
Trial 4	-	-	0.616	0.364	0.54	0.336	0.184	0.188
Trial 5	-	-	0.742	0.351	0.543	0.485	0.241	0.106
Min	0.425	0.482	0.401	0.194	0.385	0.176	-0.136	0.106
Max	0.458	0.519	0.742	0.399	0.549	0.497	0.241	0.256
Average	0.446	0.495	0.58	0.313	0.506	0.35	0.102	0.183
Std. dev.	0.018	0.021	0.142	0.084	0.069	0.14	0.144	0.066

I. Subject 9

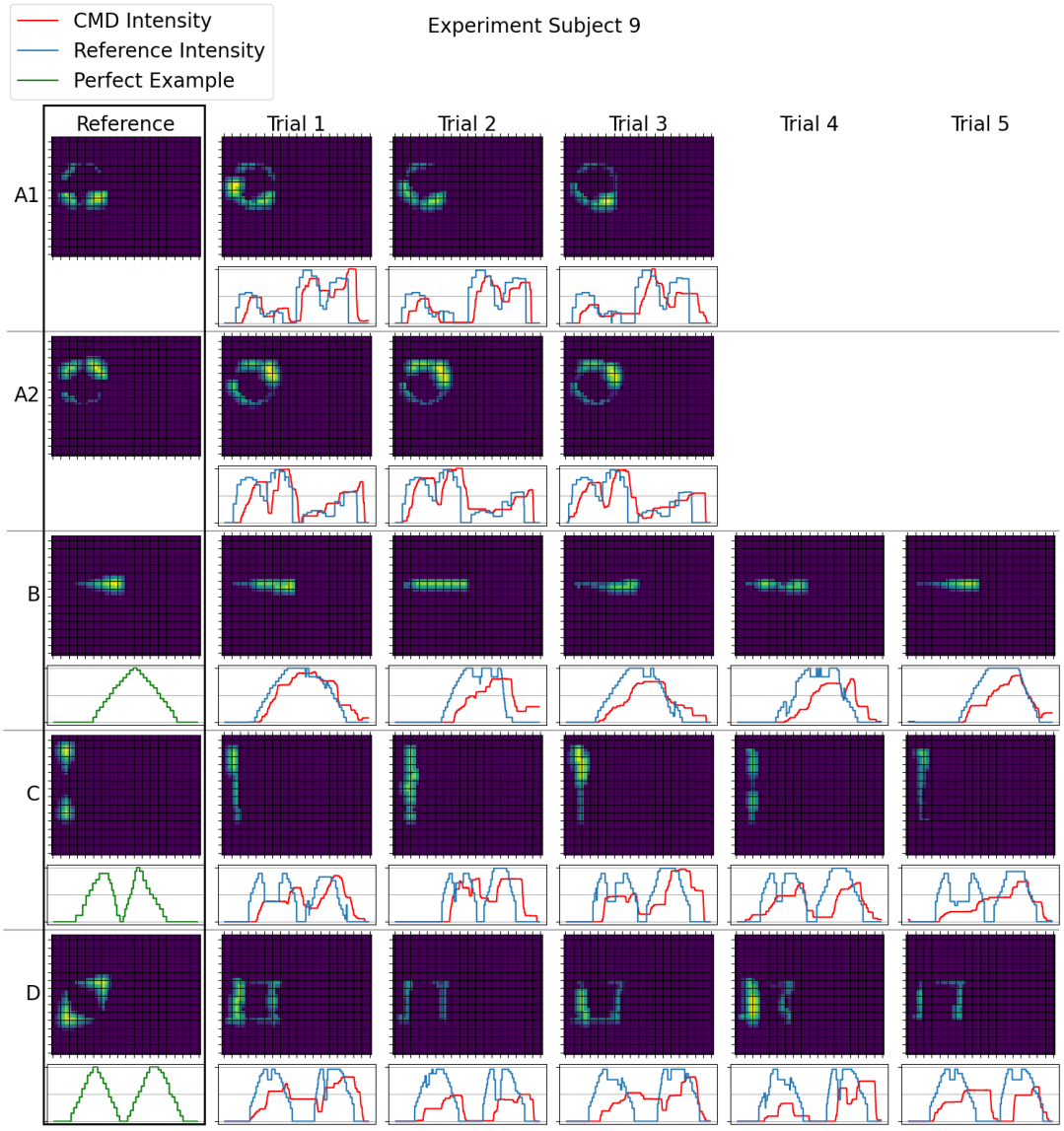

Fig. G.9: Discomfort maps and plots of reference intensity vs subject commanded intensity over time for subject 9.

TABLE G.9: Intensity and map scores for subject 9.

	Intensity					Map		
Reference	A1	A2	B	C	D	B	C	D
Trial 1	0.35	0.401	0.72	0.324	0.38	0.506	0.156	0.176
Trial 2	0.464	0.426	0.39	0.347	0.257	0.252	-0.076	0.144
Trial 3	0.435	0.409	0.555	0.34	0.318	0.428	-0.0	0.12
Trial 4	-	-	0.441	0.422	0.216	0.317	0.161	0.032
Trial 5	-	-	0.595	0.401	0.286	0.685	0.189	0.128
Min	0.35	0.401	0.39	0.324	0.216	0.252	-0.076	0.032
Max	0.464	0.426	0.72	0.422	0.38	0.685	0.189	0.176
Average	0.416	0.412	0.54	0.367	0.292	0.438	0.086	0.12
Std. dev.	0.059	0.013	0.131	0.042	0.062	0.169	0.117	0.054

J. Subject 10

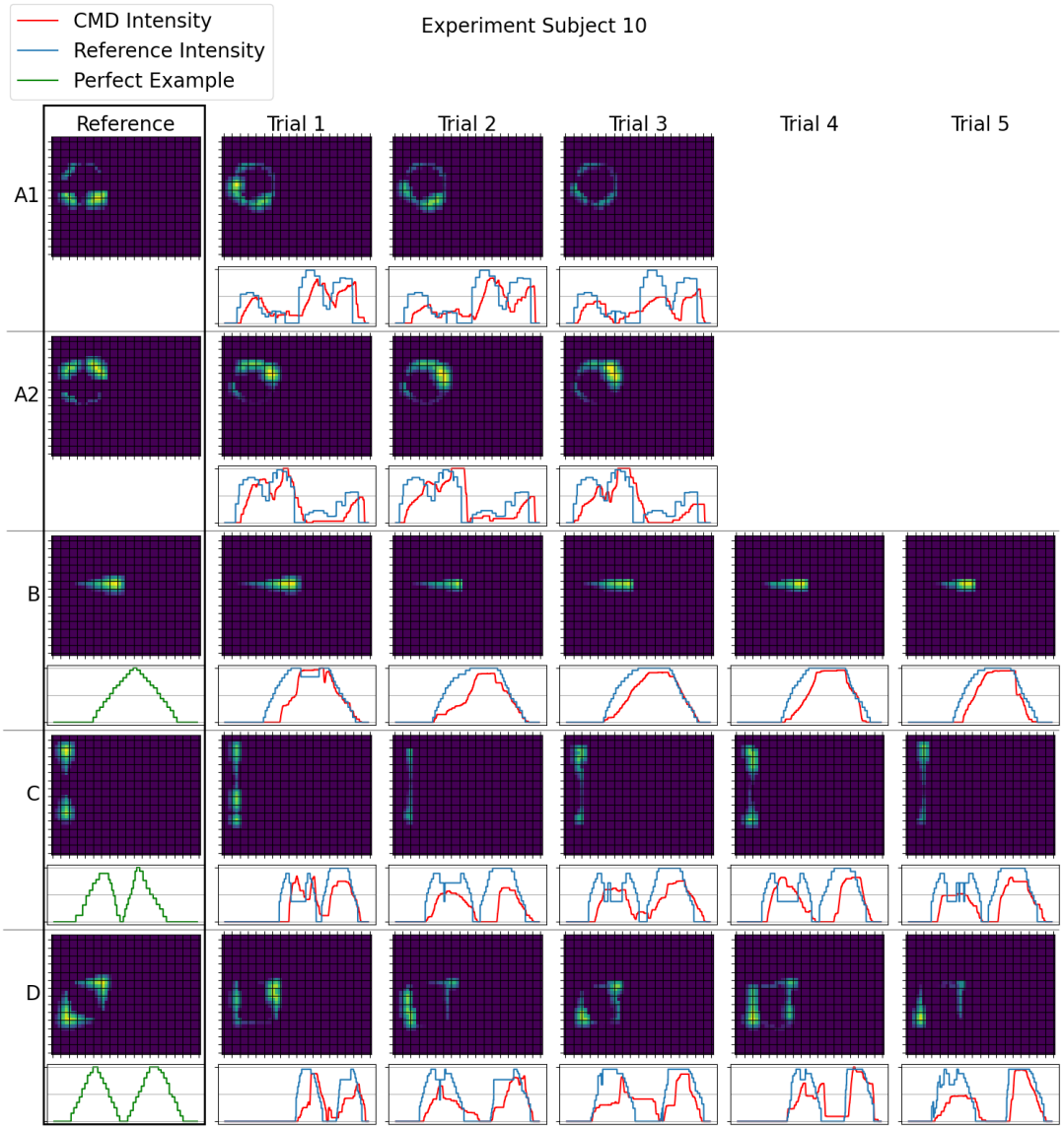

Fig. G.10: Discomfort maps and plots of reference intensity vs subject commanded intensity over time for subject 10.

TABLE G.10: Intensity and map scores for subject 10.

	Intensity					Map		
Reference	A1	A2	B	C	D	B	C	D
Trial 1	0.475	0.484	0.572	0.434	0.384	0.536	0.348	0.207
Trial 2	0.421	0.418	0.601	0.388	0.484	0.549	0.219	0.239
Trial 3	0.395	0.44	0.699	0.452	0.422	0.642	0.352	0.364
Trial 4	-	-	0.663	0.357	0.499	0.649	0.312	0.203
Trial 5	-	-	0.693	0.494	0.521	0.599	0.296	0.288
Min	0.395	0.418	0.572	0.357	0.384	0.536	0.219	0.203
Max	0.475	0.484	0.699	0.494	0.521	0.649	0.352	0.364
Average	0.43	0.447	0.646	0.425	0.462	0.595	0.305	0.26
Std. dev.	0.041	0.033	0.056	0.054	0.057	0.052	0.054	0.067